Developing and optimizing allele specific antisense oligonucleotide for KCNQ4-related autosomal dominant hearing loss

Seung Hyun Jang

The Graduate School
Yonsei University
Department of Medicine

Developing and optimizing allele specific antisense oligonucleotide for KCNQ4-related autosomal dominant hearing loss

A Dissertation Submitted
to the Department of Medicine
and the Graduate School of Yonsei University
in partial fulfillment of the
requirements for the degree of
Doctor of Philosophy in Medical Science

Seung Hyun Jang

December 2024

This certifies that the Dissertation of Seung Hyun Jang is approved

Thesis Supervisor Heon Yung Gee

Thesis Committee Member Jinwoong Bok

Thesis Committee Member Jinsei Jung

Thesis Committee Member Jinkuk Kim

Thesis Committee Member Yeonjoon Kim

The Graduate School
Yonsei University
December 2024

ACKNOWLEDGEMENTS

First, I would like to thank my thesis supervisor, pf. Heon Yung Gee, who has been always encouraging and enthusiastic about this study. Since I did not have a strong background for molecular genetics, his insightful comments and guidance helped me tremendously in fulfilling my degree and completing my dissertation. Additionally, I would like to thank all the other thesis committee members, including pf. Jinwoong Bok, Jinsei Jung, Jinkuk kim, and Yeonjoon Kim, for their constructive advice, which considerably strengthened my work.

I am grateful to all my lab members for their assistance, especially Jae Won Roh for conducting the electrophysiologic experiments to assess outer hair cell function from ex-vivo cochlea. Importantly, I would like to express heartful gratitude to my wife, Yeojeong Seo, for her unwavering support throughout my degree. Furthermore, I wish to thank my parents and my sister, who have always encouraged and supported me to endure all setbacks.

TABLE OF CONTENTS

LIST OF FIGURES

LIST OF TABLES

ABSTRACT

Developing and optimizing allele specific antisense oligonucleotide for KCNQ4-related autosomal dominant hearing loss

Hearing loss is the most common sensory organ disorder. Genetic mutations are a significant cause of hearing loss, with over 150 genes identified as causative when mutated. KCNQ4, a voltage-gated potassium channel, is highly expressed in cochlear outer hair cells, and mutations in KCNQ4 have been reported to cause progressive hearing loss (DFNA2), making it the most common deafness-causing autosomal dominant gene among East Asians. Among the many pathogenic mutations in KCNQ4 responsible for hearing loss, KCNQ4 p.W276S (c.G827C) mutation is one of the frequent dominant-negative mutations associated with DFNA2. Despite this prevalence, there is no effective biological treatment for KCNQ4-associated hearing loss, highlighting an imperative clinical need for novel therapeutics. Here, we employed allele-specific antisense oligonucleotides (ASO) to target and develop novel therapeutics for the dominant-negative KCNQ4 mutation.

Through in *vitro* screening, we identified that two out of the nine ASOs (ASO-123 and -127) selectively targeted the mutant mouse Kcnq4, while sparing the WT, in a dose-dependent manner. Considering toxicity profiles, we selected ASO-123 as the final candidate. For the in *vivo* experiment, we generated a Kcnq4 p.W277S knock-in mouse harboring a homologous mutation to human KCNQ4 p.W276S. This model successfully recapitulated progressive hearing loss and deterioration of outer hair cells, particularly at high frequencies. NGS and RT-PCR of ASO-123 injected cochleae in Kcnq4 p.W277S heterozygous mutant mice indicated preferential knockdown of mutant transcripts over wild-type, while the injection in wild-type mice did not induce hearing loss, suggesting the safety of ASO-123. Serial audiological tests corroborated the observed efficiency in transcript levels, mitigating progressive hearing loss up to 7 weeks post-injection with improved survival and function of outer hair cells. Transcriptomic analyses further validated the therapeutic efficacy and safety of ASO-123 in the inner ear.

Our findings suggest that tailored ASO targeting a dominant-negative mutation can ameliorate progressive hearing loss. Further optimization is expected to increase safety and the potential for

clinical translation.

Key words : Hearing loss; Inner ear; Autosomal dominant; Antisense oligonucleotides

I. INTRODUCTION

Hearing loss affects over 5% of the global population [1], with genetic factors responsible for more than 50% of congenital [2] and about 30-40% of post-lingual cases [3]. Despite the identification of over 150 genes linked to hearing loss, there are currently no approved biological treatments for genetic hearing loss.

Mutations in the *KCNQ4* gene cause autosomal dominant, non-syndromic hearing loss (DFNA2; deafness, autosomal dominant 2A) and account for a substantial fraction of autosomal dominant hereditary hearing loss[4]. *KCNQ4* encodes a voltage gated potassium channel (Kv7.4) primarily located on the basolateral surface of cochlea outer hair cells (OHC), playing a crucial role in OHC replolarization through potassium efflux [5]. In mice, biallelic knock out of the *Kcnq4* gene results in progressive hearing loss and selective OHC degeneration, underscoring its importance in normal hearing [6]. While some *KCNQ4* variants cause hearing loss through gain-of-function [7] or haploinsufficiency [8], most variants act through a dominant-negative effect, where mutant KCNQ4 disrupts wild-type (WT) KCNQ4 function [4,9]. The c.827G>C; p.W276S mutation is a common dominant-negative mutation and a mutational hot spot in the *KCNQ4* gene [9-11]. Our previous studies showed that *Kcnq4* p.W277S knock-in mice, which carry the homologous mutation to human *KCNQ4* p.W276S, exhibit progressive hearing loss with OHC degeneration, confirming the pathogenecity of this mutation [12].

Advances in understanding the mechanisms of genetic hearing loss, along with the development of AAV serotypes and promoter systems that enable precise transgene expression in specific cell types, have made AAV-based gene replacement therapy successful in many preclinical models and even in humans[13-17]. However, this approach is ineffective for hearing loss caused by dominant-negative or gain-of-function mutations. CRISPR/Cas9 holds promise for treating these mutations [12,18,19], but safety concerns persist, such as off-target editing in genomic DNA [20,21], the potential formation of large structural variants or integration of AAV viral genomes at the target site [22-24], immune responses to AAV vectors [25], and neutralizing antibodies to AAV that may reduce treatment efficacy or limit repeated dosing [13,26].

Antisense oligonucleotides (ASOs) are single-stranded, chemically modified oligonucleotides that have been effectively used in various neurological disorders to modify cryptic splicing events

[27-29] or degrade mutant alleles via RNase-H1 [30-33], offering high target specificity and low toxicity. While splice-switching ASOs have shown success in treating hearing loss in a mouse model of Usher syndrome [34,35], the potential of allele-specific ASOs to target dominant-negative heterozygous mutations remains largely unexplored.

In this study, we utilized allele-specific ASOs to create a new therapeutic approach targeting a dominant-negative *Kcnq4* mutation. The efficacy of these ASOs was evaluated in the inner ear using a previously established *Kcnq4* p.W277S mouse model [12]. By selectively reducing mutant transcript levels while preserving WT transcripts using allele-sepcific ASO, we observed an improvement in progressive hearing loss for up to 7 weeks post-injection, accompanied by enhanced OHC survival and function. Overall, these results offer a comprehensive strategy for developing allele-specific ASOs targeting other dominant-negative or gain-of-function mutations associated with hereditary hearing loss, with potential for clinical application.

II. MATERIALS AND METHODS

1. Antisense Oligonucleotides

The gapmer with 2'-O-methoxyethyl (2'-MOE) modification and all phosphorothioate backbone were synthesized and purifed by QMINE. 5'-methylcytosine was used instead of cytosine. The reconstitution of the oligonucleotides was done with sterile, filtered PBS (Thermo Fisher, Cat #10010023) in a sterile-hood and stored at -20 ℃ until use. The sequence and chemistry of oligonucleotides used in this study are presented in Table 1.

2. Plasmid construction

The cDNA of mouse *Kcnq4* (MR223106) and human *KCNQ4* (RC220242) was purchased from OriGene Technologies and subcloned into the pENTR-D-TOPO vector (Invitrogen, Cat #K240020). LR clonase (Invitrogen, Cat #11,791,019) was used for mammalian expression vector construction, following the provided manufacturer's instructions, with an N-terminal FLAG-or Myc-tag. The mouse *Kcnq4* p.W277S and human *KCNQ4* p.W276S mutant clone was generated via PCR-based site-directed mutagenesis using the Quick Change-II XL site-directed mutagenesis kit (Agilent Technologies, Cat #200,521).

3. Cell culture and transfection

HEK293T or HeLa cells were cultured in Dulbecco's modified essential medium (DMEM; Gibco BRL, Cat #11,965,092) supplemented with 10% fetal bovine serum (FBS; Sigma, Cat #F2442) and penicillin (50 IU/ml)-streptomycin (50 μg/ml) (Gibco BRL, Cat #GIB-15410-122) at 37 ℃ in a 5% CO2 incubator. Transfection of plasmids and ASO was performed using Lipofectamine 2000 (Invitrogen, Cat #11,668,019) following the manufacturer's instructions. ASO doses were determined based on the final concentration in the culture medium.

4. Immunoblotting

Immunoblotting was performed as described previously [36]. Briefly, forty-eight hours after transfection, protein samples were harvested and suspended in a sodium dodecyl sulfate (SDS)

buffer, then separated by SDS-polyacrylamide gel electrophoresis. The separated proteins were transferred to a nitrocellulose membrane and blotted with appropriate primary and secondary antibodies: Anti-FLAG primary antibody (1:1000, Cell Signaling Technology, Cat #8,146), Anti-Myc primary antibody (1:1000, Cell Signaling Technology, Cat #2276S), HRP Anti-β-actin primary antibody (1:2000, Abcam, Cat #ab49,900), and HRP anti-isotype secondary antibody (1:2000, Cell Signaling Technology, Cat #7076P2). Protein band signals were captured using Super Signal West-Pico Kit (Thermo Scientific, Cat #34,579), and band intensities were quantified using ImageJ.

5. In *vitro* ASO toxicity assay

We employed Caspase-Glo 3/7 assay (Promega, Cat#G8090) for high-throughput analysis of caspase activation by ASOs. Briefly, HeLa cells were seeded in a 96-well plate, transfected with specified concentrations of ASOs, and incubated for 8 hours. After incubation, equal volume of Caspase-Glo 3/7 reagent was directly added to the wells and luminescence was recorded after 30 minutes using a Centro XS^3 LB 960 Microplate Luminometer (Berthold). Background signals were determined from wells only containing medium without cells and the average of background signals were subtracted from the signals from ASO or mock treated wells. Relative caspase activity was calculated as the signals from ASO treated samples / an average signal of mock-treated samples.

6. Off-target profiling

Subsequences of ASO-123, Nusinersen, and Inotersen were computationally generated by progressively trimming ends from full-lengths to 15 or 16-nt lengths. BWA (v.0.7.17) [37] was used to align the full-length sequence or subsequences on the reference genome of corresponding species (for ASO-123, GRCm39; for Nusinersen and Inotersen, GRCh38).

7. Mice

Animal experiments were reviewed and approved by the Institutional Animal Care and Use Committee (IACUC) of Yonsei University College of Medicine (#2020-0333). Mice were housed under pathogen-free conditions with a light cycle from 8:00 AM to 8:00 PM and had ad libitum

access to water and irradiated rodent chow (LabDiet, Cat #0006972), The generation of the *Kcnq4* p.W277S knock-in mouse model (C57BL/6N) was described previously[12]. For genotyping of mice, genomic DNA was extracted from tail cut samples, and Restriction Fragment Length Polymorphism (RFLP) analysis was carried out. Briefly, PCR was performed using appropriate primers (Kcnq4-genotype-fwd: 5'-GCATTCCTAGGGGTCTTTCC-3', Kcnq4-genotype-rev: 5´-CATCAGGT TCTTGCGAACCT-3´). After successful PCR, PCR products were digested by NdeI (NEB, Cat #R0111S) for 1-2 h at 37 ℃, and 1.5% agarose gel electrophoresis was performed to determine genotype.

8. Inner ear injection

ASOs were injected into the inner ear of *Kcnq4* p.W277S heterozygous pups at Postnatal day 1 (P1) – P3. After the pups were anesthetized by hypothermia, a post-auricular incision was made to expose the tympanic bulla. One microliter of ASO was injected into the cochlea through the round window using a glass pipette and a Nanoliter2020 Injection (World Precision Instruments, Hertfordshire, UK) at a steady rate of 250 nL/min. Following the injection, the incision was sutured with Nylon 6-0, and the pup was placed on a heating pad to fully recover consciousness for at least 10 minutes.

9. RNA extraction and RT-PCR

For RNA extraction, cochleae from mice were dissected from temporal bone and the vestibule and semicircular canal were removed. Total RNA was extracted from cochleae using TRIzol (Invitrogen, Cat #15,596,026), and 1 μg of total RNA was reverse-transcribed using the RNA to cDNA EcoDry Premix (Double Primed) kit (Takara, Cat #639,548), following the manufacturer's instructions. One microliters of the RT product were used for SYBR RT-PCR with the TB Green Premix Ex Taq II (Tli RNaseH Plus) kit (Takara, Cat #RR820A) and appropriate primers (*Kcnq4*-RT-PCR-fwd: 5'-GGAAACCCTTCTGTGTCATCGA-3', *Kcnq4*-RT-PCR-rev: 5'-TGTGCCCGCAGCTATCACT-3, *Actb*-RT-PCR-fwd: 5'-GAGACCTTCAACACCCCAGC-3', *Actb*-RT-PCR-rev: 5'-ATGTCACGCACGATTTCCC-3'). The $2^{-\Delta\Delta CT}$ method was utilized for relative quantification during RT-PCR data analysis, with *Actb* serving as the housekeeping gene.

10. RNA sequencing

After dissecting the cochlea from the temporal bone, with the vestibule and semicircular canals removed, total RNA was extracted from homogenized samples using the QIAzol lysis reagent (Cat #79306; Qiagen, Hilden, Germany) while clean-up was conducted using a RNeasy mini kit (Cat #74106; Qiagen), following the manufacturer's instructions. Total RNA concentration was calculated using Quant-IT RiboGreen (Cat #R11490; Invitrogen). To assess the integrity of the total RNA (RIN), samples were run on the TapeStation RNA screentape (Cat #5067-5576; Agilent Technologies). Only high-quality RNA preparations, with RIN values greater than 7.0, were used for RNA library construction. RNA sequencing was performed at Macrogen (Seoul, Korea). A library was independently prepared with 1 μg of total RNA for each sample using the Illumina TruSeq stranded mRNA sample prep kit (Cat #RS-122-2101; Illumina, Inc.). The poly-A containing mRNA molecules were purified using poly-T-attached magnetic beads. Following purification, the mRNA was fragmented into small pieces using divalent cations under elevated temperature. The cleaved RNA fragments were copied into first strand cDNA using SuperScript II reverse transcriptase (Cat #18064014; Invitrogen) and random primers. This was followed by second strand cDNA synthesis using DNA polymerase I, RNase H, and deoxynucleotide triphosphate. These cDNA fragments underwent an end-repair process, addition of a single "A" base, and ligation of adapters. The products were then purified and PCR-enriched to create the final cDNA library. The libraries were quantified using KAPA library quantification kits for Illumina sequencing platforms according to the qPCR quantification protocol and qualified using the TapeStation D1000 ScreenTape (Cat# 5067-5582; Agilent Technologies). Indexed libraries were then submitted to an Illumina NovaSeq 6000 (Illumina, Inc.) platform, and 2 × 101 bp paired-end sequencing was performed.

Raw sequencing quality was assessed using FastQC (v0.12.1), and adapter trimming and quality filtering were conducted using Trimmomatic (v0.40) [38]. Reads were aligned to GRCm39 with HISAT2 (v2.2.1) [39], retaining only uniquely mapped reads. Total exon reads were counted by FeatureCounts (v2.0.6) [40]. Downstream analyses were performed in R (v4.2.1). Differential gene expression and Gene Ontology analysis were conducted with DESeq2 (v1.38.3) [41] and ClusterProfiler (v4.6.2) [42], respectively. For Gene Set Variation Analysis (GSVA), GSVA package (v1.46.0) [43] was used. Genes related to potassium ion transport (GO:0006813) were obtained from

the MSigDB database (https://www.gsea-msigdb.org/gsea/msigdb), while genes associated with hearing maintenance were acquired from a previous publication [44].

11. Targeted deep-sequencing

Total RNA was extracted from the cochleae, and cDNA synthesis was conducted following the methods described above. Amplification of target site sequences was carried out using *Kcnq4*-deep-seq-fwd (5'-ACACTCTTTCCCTACACGACGCTCTTCCGATCTTATGCGCACAGTAAGGAGCT-3') and *Kcnq4*-deep-seq-rev (5'-GTGACTGGAGTTCAGACGTGTGCTCTTCCGATCTGCAGGGCAAAGAAGGAGATG-3'). Subsequently, PCR products were observed on 1.5% agarose gels and purified using a Tiagen purification kit (Cat #4,992,197). Paired-end reads of 150 base pairs were generated using an Illumina Novaseq 6000 platform. Data analysis of the original sequencing fastq files was conducted with Cutadapt[45] and DADA2[46]. Firstly, adaptor and primer sequences were trimmed using Cutadapt. Subsequently, low-quality reads were filtered out, and forward and reverse reads were merged. Chimeric reads were then removed to generate the final amplicon sequence variants (ASVs) table using DADA2. For the calculation of read counts, the WT sequence without the upstream synonymous mutation (5'-CCTATGCCGACTCGCTCTGGTGGGGG-3') or the mutant sequence with the upstream synonymous mutation (5'-CATATGCCGACTCGCTCTGGTCGGGG-3') were counted in the final ASVs table.

12. ABRs and DPOAEs

ABR thresholds were assessed in a sound-proof chamber using Tucker-Davis Technologies (TDT) RZ6 digital signal processing hardware and BioSigRZ software (Alachua, FL, USA). Electrodes were positioned at the vertex and ventrolateral to both ears of anesthetized mice. Click and tone burst stimuli were generated at different frequencies (6, 12, 18, 24, and 30 kHz) using SigGenRZ software and an RZ6 digital signal processor. These stimuli were delivered to the ear canal using a multi-field 1 (MF1) magnetic speaker (TDT). The stimulus intensity was varied from 20 to 90 dB SPL in 5 dB increments. The ABR signals were then fed into a low-impedance Medusa Biological Amplifier System (RA4LI, TDT), which sent the signals to the RZ6 digital signal processing hardware. The recorded signals were filtered with a 0.5-1 kHz band-pass filter, and the ABR

waveforms in response to 512 tone bursts were averaged. BioSigRZ software was used to determine ABR thresholds for each frequency, and peak amplitudes (mV) were calculated using click-evoked ABR waveforms as input/output (I/O) functions with an increasing stimulus level (20-90 dB SPL).

For DPOAE measurements, a combination of TDT microphone-speaker systems was used. Primary stimulus tones were generated using an RZ6 digital signal processor with SigGenRZ software and delivered through a custom probe with an ER 10B+ microphone (Etymotic, IL, USA) and MF1 speakers placed in the ear canal. The primary tones had a frequency ratio (f2/f1) of 1.2, and target frequencies included 6, 12, 18, 24, and 30 kHz. The intensity of f2 was the same as f1 (L1 = L2). The resulting sounds from the primary tones were recorded using an RZ6 digital signal processor. DPOAE input/output (I/O) functions were determined at specific frequencies with an f2/f1 ratio of 1.2 and L1 = L2. The intensity of the primary tones was increased from 20 to 80 dB SPL in 5 dB SPL increments. Fast Fourier Transform was performed for each primary tone using DP-grams, and for the I/O function intensity, BioSigRZ software was used to determine the average spectra of the two primaries, 2f1 – f2 distortion products, and noise floor.

13. Immunofluorescence and confocal microscopy

The inner ear tissues dissected from mice temporal bone were fixed in 4% paraformaldehyde (PFA) in PBS at 4°C for overnight. The fixed cochleae were decalcified with 500mM EDTA (iNtRON, Cat#IBS-BE002). Then, samples were microdissected to separate organ of Corti from three turns (apex: 6-8kHz region; mid: 16-18kHz region; base: 30kHz region) under microscope and simultaneously permeabilized and blocked with 5% donkey serum (Sigma, Cat #D9663), 0.1% BSA (Sigma, Cat #A7030), and 0.1% Triton X-100 (Biosesang, Cat#TR1020-500) in PBS for 1 hour at room temperature. Anti-Myo7a primary antibody (Proteus, Cat #PTS-25-6790) or Anti-fluorescein primary antibody (Abcam, Cat#ab19491) were diluted 1:200 and incubated 4°C for overnight. After three times washing with PBS, fluorophore-tagged secondary antibodies were diluted 1:500 and incubated for 2 hours at room temperature. After secondary antibody incubation, samples were washed three times with PBS and mounted on the slide glass with fluorescence mounting medium (Dako, Cat#S3023). Z-stacked confocal images were obtained using Carl Zeiss LSM780 microscopes while images were processed using ZEN software.

14. Statistical analyses

Statistical differences between two groups were analyzed using Student's t-test. For comparisons involving more than two groups, one-way or two-way analysis of variance (ANOVA) was performed with appropriate corrections for multiple comparisons as specified in each figure legend, using the GraphPad Prism 8.0 software (GraphPad Software, CA, USA). Two-sided p values of less than 0.05 were considered significant. All data in figures were presented with mean ± standard deviations (SDs) or standard errors (SEs).

III. RESULTS

1. In *vitro* screening of candidate allele-specific ASOs targeting the Kcnq4 p.W277S mutation

To target the *Kcnq4* p.W277S mutation, we designed several gapmer ASOs, each 16-18 nucleotides (nt) long, with all phosphorothioate bonds and 2'-MOE modifications at the sugar's 2' position on both the 3' and 5' ends (Figure 1A and Table1). These ASOs induce target transcript knockdown through RNase-H1-mediated degradation [47]. To assess the potency and selectivity of the ASOs, we co-transfected HEK293T cells with either Kcnq4 p.W277S or WT plasmids and one of the candidate ASOs, and measured protein expression after 48 hours as the endpoint of treatment. Compared to the non-targeting scrambled ASO (NT-ASO), several ASOs effectively knocked down the Kcnq4 p.W277S (Figure 1B), with some showing strong selectivity against the WT Kcnq4 (Figure 1C). To statistically compare the allele discrimination capacity of these ASOs, a two-way ANOVA test was conducted to measure the impact of different ASOs and alleles on expression levels (Figure 1D). Consequently, we identified two ASOs (ASO-123 and -127) that demonstrated significantly stronger suppression of mutant Kcnq4 expression compared to WT Kcnq4 at a 50nM concentration.

To assess the dose-dependent potency and selectivity of the two promising ASOs (ASO-123 and -127), we treated cells with different concentrations of each ASO and measured the target protein expression levels (Figure 2A-D). Both ASO-123 and -127 effectively inhibited the expression of mutant Kcnq4 protein in a dose-dependent manner, exhibiting similar potency (half-maximal inhibitory concentrations (IC_{50}) for ASO-123: 16.24nM; IC_{50} for ASO-127: 16nM). Additionally, regarding selectivity, ASO-123 also outperformed ASO-127, showing an IC_{50} of 61.99nM compared to 29.38nM for ASO-127. We calculated the ratio of IC_{50} for the Kcnq4 WT and W277S proteins in ASO-123 and -127 as another marker for allele discrimination capacity, revealing that ASO-123 exhibited 2.08-fold greater selectivity than ASO-127 (IC_{50} for WT / IC_{50} for W277S; for ASO-123: 3.82; for ASO-127: 1.84). Overall, these findings indicate that ASO-123 offers a potent and selective reduction of the *Kcnq4* W277S allele with approximately 3.82-fold higher affinity for the mutant allele over WT in vitro.

Given that ASOs with phosphorothioate bonds may cause toxicity via caspase-mediated apoptosis [48], we transfected HeLa cells with ASO-123, -127, NT-ASO, or a known toxic ASO (ASO-tox) [48] at various concentrations and evaluated caspase-3/7 activation to address potential safety concerns for in vivo experiments (Figure 2E). Consistent with prior findings, ASO-tox resulted in approximately 2.5-fold higher activation of caspase-3/7 at 800nM compared to mock-treated samples. Notably, ASO-127 also triggered similar levels of caspase activation as ASO-tox. In contrast, ASO-123 and NT-ASO showed significantly lower caspase-3/7 activation compared to ASO-tox-treated samples, even at 800nM — a concentration 49.26 times higher than the IC_{50} of ASO-123 for Kcnq4 W277S. Lastly, we analyzed the off-target profile of ASO-123 and determined that it has a comparable or even cleaner off-target profile in the mouse genome compared to FDA-approved ASOs (Nusinersen[49]: splice-switch ASO, Inotersen[50]: gapmer ASO, Table 2-4). Collectively, these findings indicate that ASO-123 has a safer profile than ASO-127 and is appropriate for further in vivo experiments.

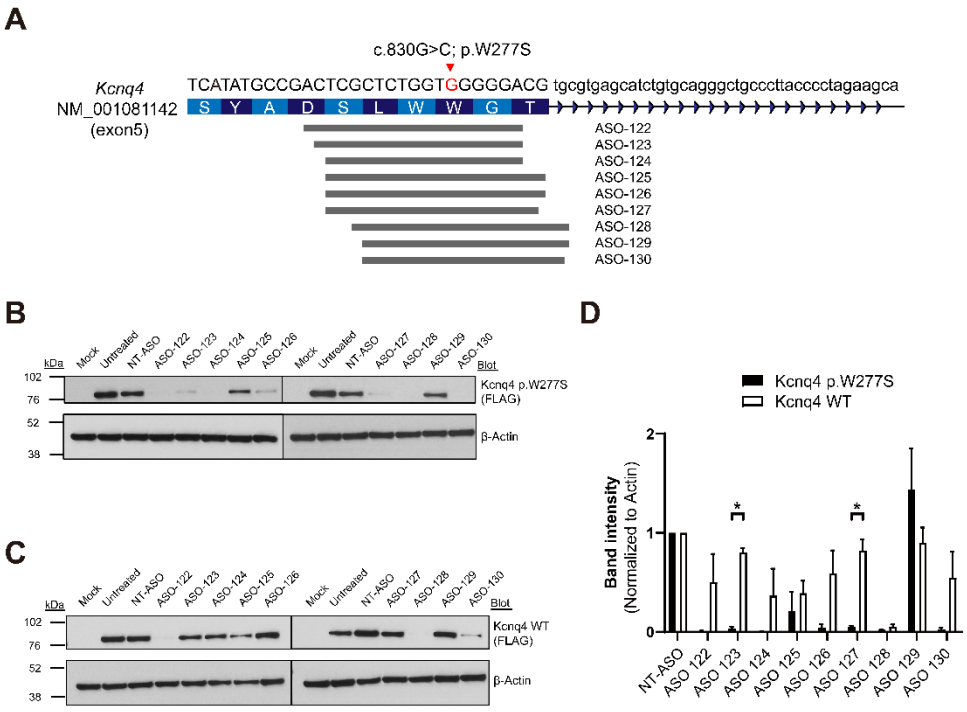

Figure 1. In *vitro* screening of candidate ASOs. (a) Schematic alignment of 9 candidate ASOs that target the Kcnq4 W277S mutation. The full sequences and chemical modifications of these ASOs are presented in Table 1. (b-c) Representative western blot images assessing the potency (b) and selectivity (c) of the 9 candidate ASOs. (d) Kcnq4 W277S or WT protein band intensities normalized to β-Actin (n=3 for each treatment). Data are shown as mean ± SEs. Two-way ANOVA with Bonferroni's multiple comparison corrections were conducted to determine statistical significance. * $P < 0.05$.

Table 1. ASO sequence and chemistry. Bold indicates 2'-MOE modification; * indicates phosphorothioate bond; FAM indicates 6'-fluorescein amidites modification; For in *vivo* experiments, 5'-methyl cytosine was used instead of cytosine.

ID	Sequence (5' > 3')
ASO-122	**T*C*C*C***C*G*A*C*C*A*G*A***G*C*G*A*G*T**
ASO-123	**T*C*C*C***C*G*A*C*C*A*G***A*G*C*G*A*G**
ASO-124	**T*C*C***C*C*G*A*C*C*A***G*A*G*C*G*A**
ASO-125	**C*G*T*C*C***C*C*G*A*C*C*A***G*A*G*C*G*A**
ASO-126	**C*G*T*C*C***C*C*G*A*C*C*A*G***A*G*C*G*A**
ASO-127	**G*T*C*C***C*C*G*A*C*C*A***G*A*G*C*G*A**
ASO-128	**A*T*C*G*T*C***C*C*C*G*A*C*C*A***G*A*G*C**
ASO-129	**A*T*C*G*T*C***C*C*C*G*A*C*C***A*G*A*G**
ASO-130	**T*C*G*T*C*C***C*C*G*A*C*C*A***G*A*G**
ASO-tox	**A*A*T*G*T***G*C*C*T*G*C*T*G*T*C***C*T*T*G*A**
NT-ASO	**C*C*T*T*C***C*C*T*G*A*A*G*G*T*T***C*C*T*C*C**
FAM-NT-ASO	FAM-**C*C*T*T*C***C*C*T*G*A*A*G*G*T*T***C*C*T*C*C**

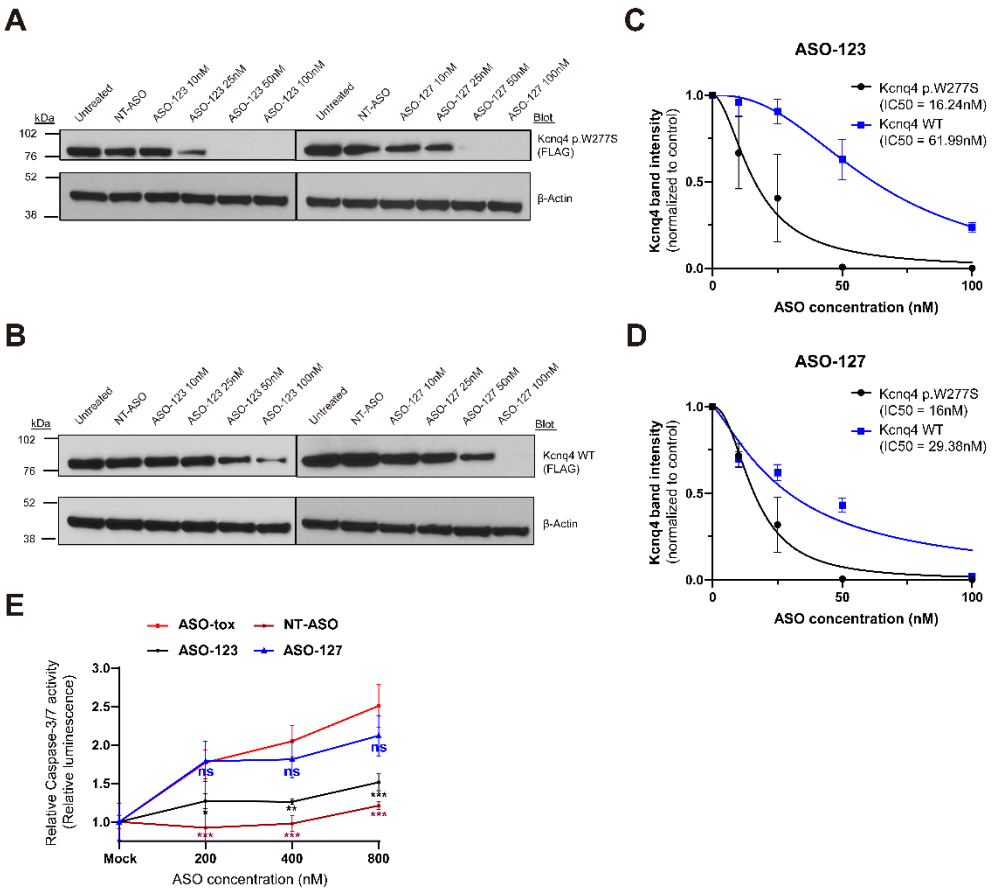

Figure 2. Dose-response and toxicity profiles of ASO-123 and -127. (a-b) Representative western blot images following treatment with NT-ASO (100nM), ASO-123 or -127 in various concentration ranges for Kcnq4 W277S (a) or WT (b). (c-d) Dose-response curves of ASO-123 (c) and ASO-127 (d) for Kcnq4 W277s or WT, normalized to β-Actin and then to naive controls (n=3). Data are presented as mean ± SEs. (e) Relative caspase-3/7 activity in HeLa cells, normalized to mock-treated samples 8 hours after ASO transfection (n=3). Data are shown as mean ± SDs. Two-way ANOVA with Dunnett's multiple comparison corrections were conducted to determine statistical significance. ns: not significant; * $P < 0.05$; ** $P < 0.01$; *** $P < 0.001$.

Table 2. Off-target profile of ASO-123. Possible off-target locus was identified through the alignment of ASO-123 full-length sequences or subsequence to the mouse reference genome (GRCm39; mm39) with allowing 1nt internal mismatch or 1nt internal indel.

Genomic matches of ASO-123 subsequences

Length (nt)	Number of possible subsequences	Number of off-target hits[a]	Off-target locus (mm39)	Gene annotation (RefSeq)			Association with hearing loss[b]
				Gene (transcript ID)	Strand	Region	
17	1	0	-	-	-	-	
16	2	0	-	-	-	-	
15	3	0	-	-	-	-	-

Genomic matches of ASO-123 sequence allowing internal mismatches

Length (nt)	Number of mismatches	Number of off-target hits[a]	Off-target locus (mm39)	Gene annotation (RefSeq)			Association with hearing loss[b]
				Gene (transcript ID)	Strand	Region	
17	1	1	Chr13:64332481-64332497	Habp4 (NM_019986)	-	Exon7	None

Genomic matches of ASO-123 sequence allowing an internal 1nt indel

Length (nt)	Number of insertion or deletion	Number of off-target hits[a]	Off-target locus (mm39)	Gene annotation (RefSeq)			Association with hearing loss[b]
				Gene (transcript ID)	Strand	Region	
18	1 (insertion)	0	-	-	-	-	-
16	1 (deletion)	0	-	-	-	-	-

[a] off-target hits located in an inter-genic region were excluded.

[b] Association between identified off-target genes and hearing loss was determined based on the phenotype data in Mouse Genome Informatics (MGI; https://www.informatics.jax.org/) and International Mouse Phenotyping Consortium (IMPC; https://www.mousephenotype.org/)

Table 3. Off-target profile of Nusinersen. Possible off-target locus was identified through the alignment of Nusinersen full-length sequences or subsequence to the human reference genome (GRCh38, hg38) with allowing 1nt internal mismatch or 1nt internal indel.

Genomic matches of Nusinersen subsequences

Length (nt)	Number of possible subsequences	Number of off-target hits[a]	Off-target locus (hg38)	Gene annotation (RefSeq)		
				Gene (transcript ID)	Strand	Region
18	1	0	-	-	-	-
17	2	2	Chr2:150295284-150295300	LINC0818 (NR_1877171)	-	Intron2
			Chr12:129455147-129455163	TMEM132D (NM_133448)	-	Intron3
16	3	6	Chr2:150295284-150295299	LINC01818 (NR_187171)	-	Intron2
			Chr7:142217497-142217512	MGAM2 (NM_001293626)	+	Intron46
			Chr12:129455147-129455162	TMEM132D (NM_133448)	-	Intron3
			Chr13:29459670-29459685	MTUS2 (NM_001384606)	+	Intron9
			Chr15:32146950-32146965	CHRNA7 (NM_000746)	+	Intron4
			Chr20:9657649-9657664	PAK5 (NM_177990)	-	Intron2

Genomic matches of Nusinersen sequence allowing internal mismatches

Length (nt)	Number of mismatches	Number of off-target hits[a]	Off-target locus (hg38)	Gene annotation (RefSeq)		
				Gene (transcript ID)	Strand	Region
18	1	3	Chr7:142217495-142217512	MGAM2 (NM_001293626)	+	Intron46
			Chr12:112960443-112960460	NCAM1 (NM_181351)	-	Intron1
			Chr13:29459670-29459687	MTUS2 (NM_001384606)	+	Intron9

Genomic matches of Nusinersen sequence allowing an internal 1nt indel

Length (nt)	Off-target locus (hg38)	Gene annotation (RefSeq)

	Number of insertion or deletion	Number of off-target hits[a]		Gene (transcript ID)	Strand	Region
19	1 (insertion)	1	Chr20:61503412-61503430	CDH4 (NM_001794)	-	Intron2
17	1 (deletion)	2	Chr3:178704046-178704062	KCMB2 (NM_181361)	+	Intron1
			Chr11:113140403-113140419	NCAM1 (NM_181351)	-	Intron1

[a] off-target hits located in an inter-genic region were excluded.

Table 4. Off-target profile of Inotersen. Possible off-target locus was identified through the alignment of Inotersen full-length sequences or subsequence to the human reference genome (GRCh38, hg38) with allowing 1nt internal mismatch or 1nt internal indel.

Genomic matches of Inotersen subsequences

Length (nt)	Number of possible subsequences	Number of off-target hits[a]	Off-target locus (hg38)	Gene annotation (RefSeq)		
				Gene (transcript ID)	Strand	Region
20	1	0	-	-	-	-
19	2	0	-	-	-	-
18	3	0	-	-	-	-
17	4	0	-	-	-	-
16	5	1	4:167118858-167118873	SPOCK3 (NM_001040159)	+	Intron2

Genomic matches of Inotersen sequence allowing internal mismatches

Length (nt)	Number of mismatches	Number of off-target hits[a]	Off-target locus (hg38)	Gene annotation (RefSeq)		
				Gene (transcript ID)	Strand	Region
20	1	0	-	-	-	-

Genomic matches of Inotersen sequence allowing an internal 1nt indel

Length (nt)	Number of insertion or deletion	Number of off-target hits[a]	Off-target locus (hg38)	Gene annotation (RefSeq)		
				Gene (transcript ID)	Strand	Region
21	1(insertion)	0	-	-	-	-
19	1(deletion)	0	-	-	-	-

[a] off-target hits located in an inter-genic region were excluded.

2. In vivo delivery of ASO-123 preferentially knocks down mutant *Kcnq4* transcripts over WT transcripts.

To evaluate the transfection efficiency of locally administered ASO in hair cells, we injected fluorescein-NT-ASO (FAM-NT-ASO) into WT mice at Postnatal day 1 to 3 (P1-3) through the round window membrane (RWM). After 4 weeks from injection, the delivered ASOs were strongly observed in nearly all inner hair cells (IHC) and most OHCs, showing an increasing gradient from the apex to the base of the cochlea (Figure 3), consistent with a previous report [34]. Furthermore, ASOs delivered via RWM also distributes to various regions of cochlea other than hair cells, including stria vascularis and spiral ganglion, and even to multiple regions of brains, probably through cochlear aqueduct [51] (Figure 4). These data demonstrate the broad biodistribution characteristics of locally delivered ASO in the inner ear.

Next, to evaluate the in *vivo* efficiencies of ASO-123 against the Kcnq4 W277S mutation, we injectd two doses (15 μg and 30 μg) of ASO-123 and 30 μg of NT-ASO as a control into Kcnq4 W277S heterozygous mice (hereafter, *Kcnq4* $^{W277S/+}$) at P1-3 through the RWM (Figure 5A). Due to the only single nucleotide difference between the *Kcnq4* WT and W277S transcripts, we were unable to identify any primers that could specifically and reliably amplify only the *Kcnq4* W277S transcript. Therefore, we conducted targeted deep sequencing of *Kcnq4* transcripts from the injected and non-injected cochleae of *Kcnq4* $^{W277S/+}$ mice at 4weeks of age. Compared to uninjected and NT-ASO-injected cochleae, the proportion of W277S trasncripts decreased from 55.66 ± 2.41% (mean ± SDs, uninjected) and 56.13 ± 1.40% (NT-ASO) to 47.30 ± 2.16% and 46.6 ± 3.29% in ASO-123 15μg and 30μg injected cochleae, respectively (Figure 5B). We further calculated the ratio of read counts between W277S and WT and found that the ratio significantly decreased by approximately 28.64% and 30.4% in ASO-123 15μg and 30μg-injected cochleae compared to uninjected samples, respectively (Figure 5C). Additionally, we evaluated the total *Kcnq4* mRNA (including both W277S and WT transcripts) expression level to estimate the change in the total quantity of *Kcnq4* mRNA in response to ASO treatment in *Kcnq4* $^{W277S/+}$ mice. RT-PCR results suggest that NT-ASO and ASO-123 15μg injection did not induce a significant reduction in total *Kcnq4* levels, although ASO-123 30μg led to a significant decrease in total *Kcnq4* levels by 61.05 ± 3.78% (Figure 5D). Therefore, we calculated that W277S transcripts decreased by approximately 42.46% and 67.39% following ASO-123 15μg and 30μg injection, respectively, while WT transcripts were reduced by about 19.52% and 53.09% with the same respective doses

(Figure 5E). Overall, these results indicate that in vivo inner ear injection of ASO-123 markedly kncoked down the *Kcnq4* W277S transcripts while relatively preserving WT transcripts when a 15μg dose was administered.

To further evaluate the potential ototoxicity of ASO-123 in vivo, we injected ASO-123 into WT mice with the same genetic background (C57BL/6N) as *Kcnq4* $^{W277S/+}$ mice and examined their auditory function using auditory brainstem response (ABR) test at 4weeks of age. The thresholds of click and tone ABR at all tested frequencies in the 15μg and 30μg ASO-123 injected mice did not differ from those in non-injected or NT-ASO injected mice (Figure 5F), implying that ASO-123 injection did not induce hearing loss.

We then measured the survival of ASO-injected *Kcnq4* $^{W277S/+}$ pups from P1 to P7 (Figure 5G). Unexpectedly, ASO-123 30μg injection significantly imparied the survival of pups until P7, while ASO-123 15μg and NT-ASO 30μg injections exhibitied comparable survival rates with uninjected pups. Therefore, even though the exact mechanism of decreased viability in mice injected with 30μg of ASO-123 remains unclear, we hypothesize that the ASO-123 30μg injection exceeded the maximal tolerable dose. Consequently, we proceeded with further phenotype evaluation using a 15μg injection dose.

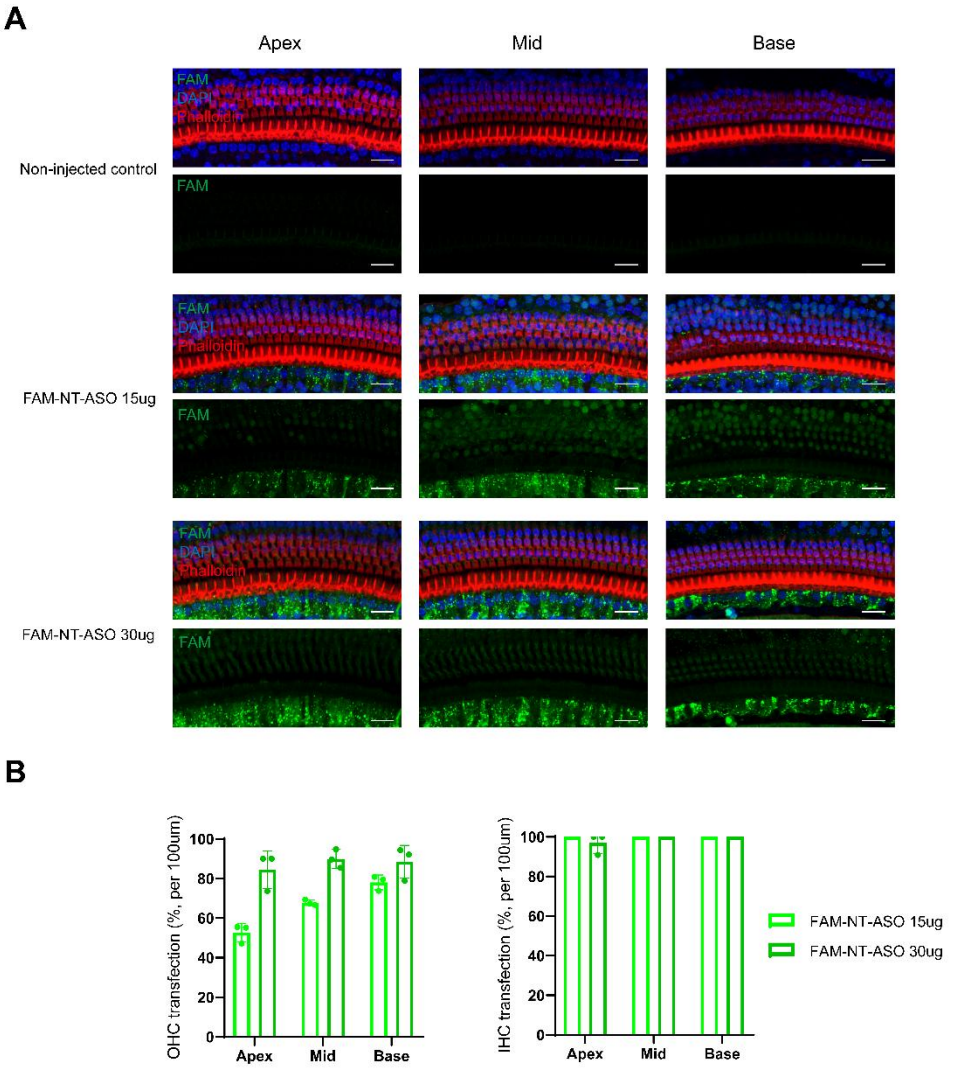

Figure 3. In vivo delivery of ASO via RWM effectively transfects hair cells. (a) Representative immunofluorescence images of ASO-injected and non-injected organ of Corti at 4 weeks post-injection. Stereocilia of hair cells were labeled with phalloidin and ASO was labeled with fluorescein amidite (FAM). Scale bar = 20 μm. (b) Transfection efficiency of OHCs (left) and IHCs (right) across apex, mid, and basal turns of cochlea. Data are shown as mean ± SDs (n=3).

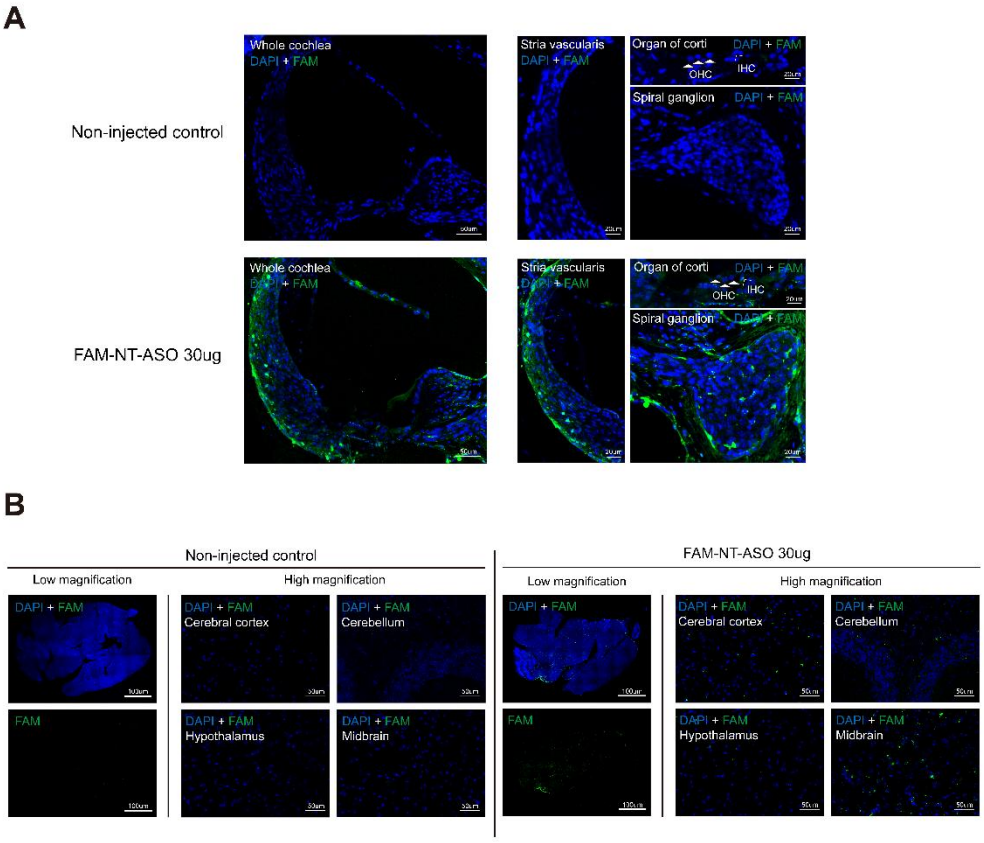

Figure 4. ASO delievered via RWM distributes to various regions of the cochlea and central nervous system. (a) Representative cross-sectional immunofluorescence images of ASO-injected and non-injected whole cochlea, stria vascularis, oragan of Corti, and spiral ganglion at 4 weeks post-injection. ASO was labeled with fluorescein amidite (FAM). Scale bar as indicated. (b) Representative sagittal immunofluorescence images of brains from ASO-injected and non-injected mice at 4 weeks post-injection. ASO was labeled with fluorescein amidite (FAM). Scale bar as indicated.

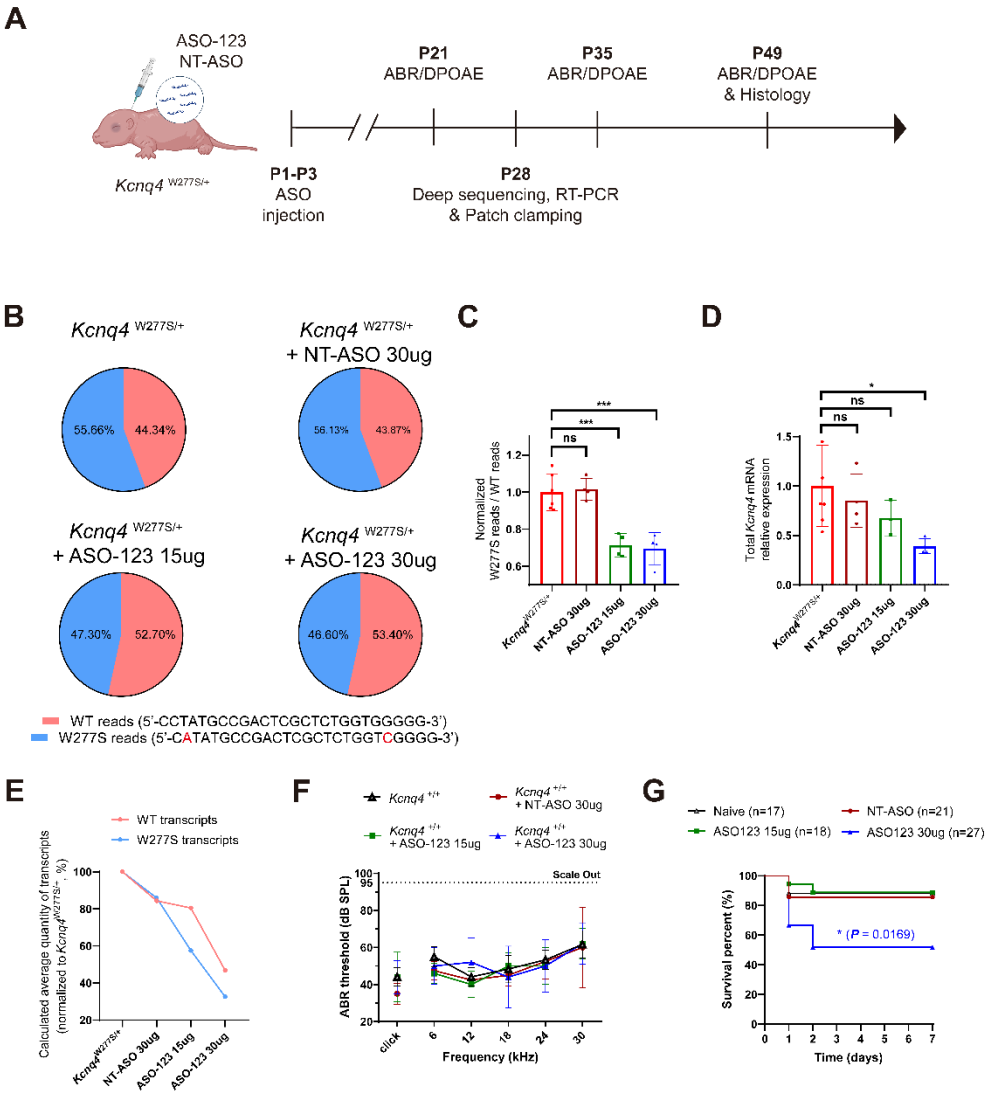

Figure 5. In vivo efficiency and safety of ASO-123 administration in the inner ear. (a) Schematic timeline of in vivo experiments. (b) Pie charts displaying the proportion of WT and W277S reads among *Kcnq4* transcripts. W277S reads were identified based on the dual presence of the W277S mutation (c.830G>C) and an upstream synonymous mutation (c.810C>A). (c) The ratio of W277S to WT read counts, normalized to uninjected samples, across the four groups. Data are presented as mean ± SDs. One-way ANOVA with Dunnett's multiple comparison corrections

was conducted to determine statistical significance. ns: not significant; * $P < 0.05$; ** $P < 0.01$; *** $P < 0.001$. (d) RT-PCR results measuring the total *Kcnq4* expression levels across the four groups. Expression levels were normalized to the *Actb* housekeeping gene and to uninjected samples. Data are presented as mean ± SDs. One-way ANOVA with Dunnett's multiple comparison corrections was conducted to determine statistical significance. ns: not significant; * $P < 0.05$; ** $P < 0.01$; *** $P < 0.001$. (e) Calculated average quantity of WT and W277S transcripts, normalized to non-injected samples, based on deep sequencing and RT-PCR results across the four groups. (f) Click and tone ABR thresholds in ASO-123 (30 μg, n= 5, blue; 15μg, n= 5, green), NT-ASO (n= 4, brown) - injected and non-injected (n= 6, black) WT mice at 4weeks of age. Data are presented as mean ± SDs. (g) Kaplan-Meier curve depicting the survival of *Kcnq4* $^{W277S/+}$ pups across the four groups until P7. A log-rank test was conducted to statistically test the difference between survival curves. ns: not significant; * $P < 0.05$.

3. ASO-123 injection ameliorates progressive hearing loss in *Kcnq4* $^{W277S/+}$ mice.

We injected 15 μg of ASO-123 into *Kcnq4* $^{W277S/+}$ mice at P1-P3 via the RWM and serially evaluated their click and tone ABR thresholds at frequencies ranging from 6kHz to 30kHz at 3, 5, and 7 weeks (Figure 6A-D). By 7 weeks, uninjected *Kcnq4* $^{W277S/+}$ mice exhibitied severe hearing loss, with mid to high frequency regions (18kHz – 30kHz) showing no discernible ABR waves upto 90 dB SPL. However, in ASO-123 injected *Kcnq4* $^{W277S/+}$ mice, there was a significant reduction in ABR thresholds in click, 6k Hz, 12k Hz, and 18k Hz tone stimuli by 12.57-25 dB SPL at 5 weeks. Furthermore, at 7 weeks, significant deceleration of progressive hearing loss was observed in click and all measured tone stimuli, with a 10.06 - 15.91 dB SPL improvement in thresholds. Additionally, we compared the wave I (P1) amplitude and latency stimlulated by 90dB SPL of click, 6, and 12 kHz tone stimuli at 7 weeks among the three groups, with 9 out of 16 untreated *Kcnq4*$^{W277S/+}$ mice excluded from analysis since no discernable wave was observed at 90dB SPL. The comparison revealed that wave I amplitudes of ASO-123 treated *Kcnq4*$^{W277S/+}$ mice in response to click stimuli significantly increased compared to untreated *Kcnq4*$^{W277S/+}$ mice and were even comparable to those in WT mice. Moreover, wave I amplitudes of ASO-123 treated mice stimulated by 6 and 12 kHz tone stimuli also showed increasing trends compared to untreated mice (Figure 7A). Similarly, wave I latency of ASO-123 treated mice displayed decreasing trends compared to non-injected *Kcnq4*$^{W277S/+}$ mice (Figure 7B).

Since Kcnq4 plays a crucial role in OHCs function, we also conducted Distortion Product Otoacoustic Emission (DPOAE) tests, which more specifically reflect OHCs function than ABR (Figure 6E-G). Serial examination of DPOAE tests revealed significant threshold improvements of 18.89 and 10.42 dB SPL in the 12k and 18k Hz frequencies at 5 weeks, with the significant difference in the 12k Hz threshold persisting until 7 weeks. Additionally, to verify that the alleviation of progressive hearing loss by ASO-123 in *Kcnq4* $^{W277S/+}$ mice was mediated by an on-target effect, we injected NT-ASO (30 μg) into the *Kcnq4* $^{W277S/+}$ mice at the same time points (P1-P3) and evaluated their auditory phenotypes. ABR and DPOAE results at 3, 5, and 7 weeks in NT-ASO injected mice indicated that hearing loss was not rescued by NT-ASO (Figure 8). Collectively, these results confirm that the preferential on-target knockdown of *Kcnq4* W277S transcripts by ASO-123 led to the amelioration of progressive hearing loss in *Kcnq4* $^{W277S/+}$ mice.

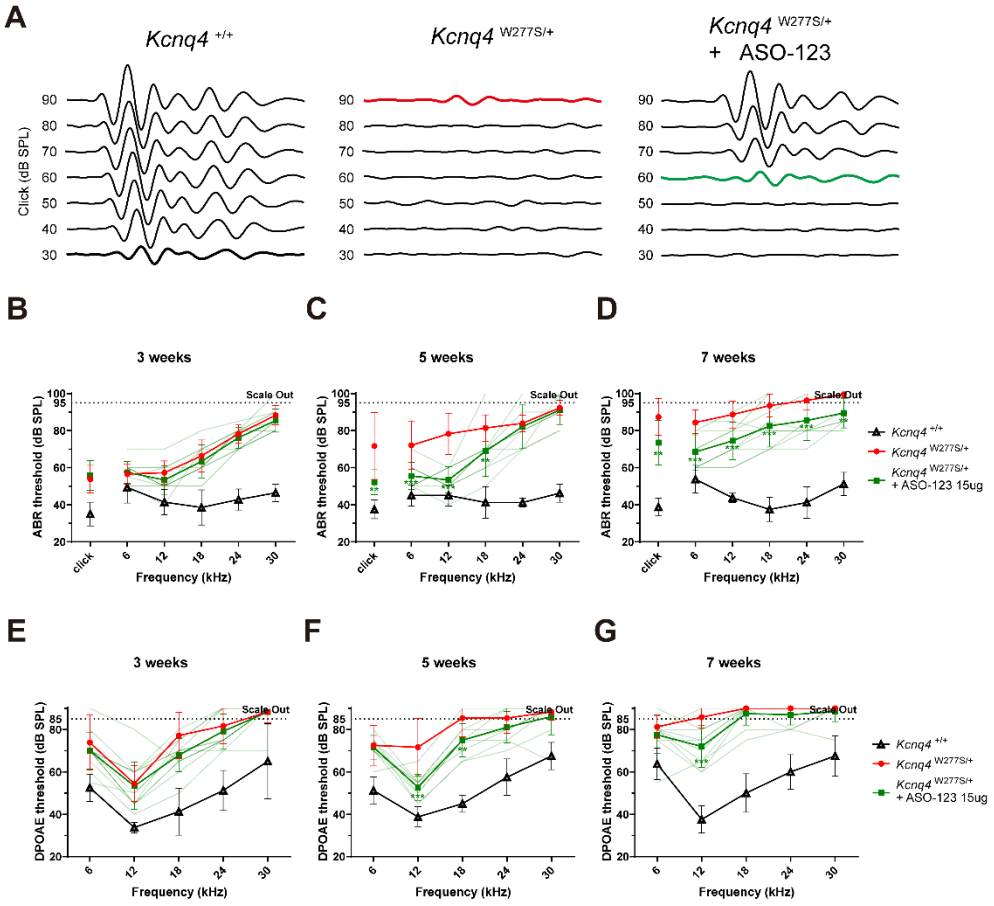

Figure 6. In vivo ASO-123 delivery alleviates progressive hearing loss in *Kcnq4* $^{W277S/+}$ mice.
(a) Representative ABR waveforms stimulated by broadband click sound in WT (*Kcnq4* $^{+/+}$), uninjected *Kcnq4* $^{W277S/+}$, and ASO-123 injected *Kcnq4* $^{W277S/+}$ mice at 7 weeks of age. Black, red, and green bold traces indicate thresholds in each group. (b-d) Average click and tone ABR thresholds at 3 (b), 5 (c), 7 (d) weeks of age in WT (n= 4), uninjected *Kcnq4* $^{W277S/+}$ (n= 16), and ASO-123 injected *Kcnq4* $^{W277S/+}$ (n= 10) mice. Transparent green lines represent thresholds from individual ASO-123 injected *Kcnq4* $^{W277S/+}$ mice. Data are shown as mean ± SDs. Two-way ANOVA tests with Bonferroni multiple comparison corrections were conducted to determine statistical significance among tone thresholds. For click threshold comparisons, one-way ANOVA tests with Bonferroni multiple comparison corrections were employed. * $P < 0.05$; ** $P < 0.01$; *** $P < 0.001$. (e-g) Average DPOA thresholds at 3 (e), 5 (f), 7 (g) weeks of age in WT (n= 4),

uninjected *Kcnq4* $^{W277S/+}$ (n= 9), and ASO-123 injected *Kcnq4* $^{W277S/+}$ (n= 10) mice. Transparent green lines represent thresholds from individual ASO-123 injected *Kcnq4* $^{W277S/+}$ mice. Data are shown as mean ± SDs. Two-way ANOVA tests with Bonferroni multiple comparison correction were conducted to determine statistical significance. * $P < 0.05$; ** $P < 0.01$; *** $P < 0.001$.

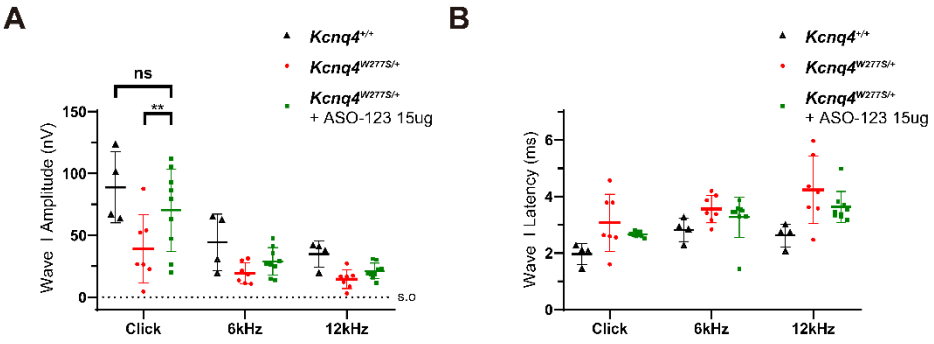

Figure 7. Wave I (P1) amplitude (a) and latency (b) in response to 90 dB SPL of click, 6-, 12-kHz tone stimuli in *Kcnq4*$^{+/+}$, ASO-123 treated, and untreated *Kcnq4* $^{W277S/+}$ mice at 7 weeks post-injection. For untreated *Kcnq4*$^{W277S/+}$ mice, 9 out of 16 mice without discernable waves in 90 dB SPL stimuli were excluded from analysis. Two-way ANOVA tests with Bonferroni multiple comparison correction were conducted to determine statistical significance. ns: not significant; ** $P < 0.01$.

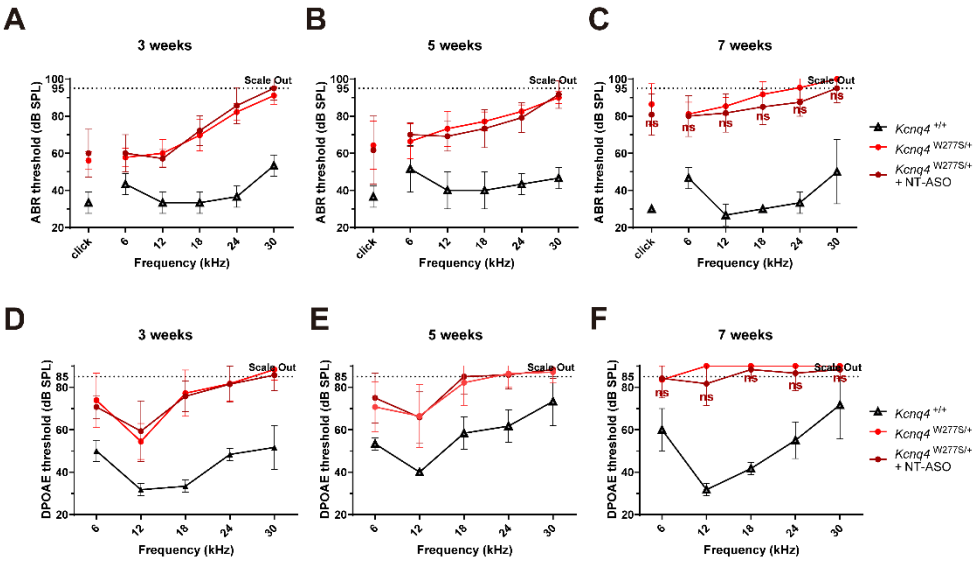

Figure 8. NT-ASO injection does not rescue hearing loss in *Kcnq4* $^{W277S/+}$ mice. (a-c) Average click and tone ABR thresholds in WT (*Kcnq4* $^{+/+}$, n= 3), uninjected *Kcnq4* $^{W277S/+}$ (n= 7), and NT-ASO injected *Kcnq4* $^{W277S/+}$ (n= 6) mice at 3 (a), 5 (b), and 7 (c) weeks of age. Data are presented as mean ± SDs. Two-way ANOVA tests with Bonferroni multiple comparison correction were conducted to determine statistical significance among tone thresholds. For click threshold comparisons, one-way ANOVA tests with Bonferroni multiple comparison corrections were used. ns: not significant. (d-f) Average DPOAE thresholds in WT (*Kcnq4* $^{+/+}$, n= 3), uninjected *Kcnq4* $^{W277S/+}$ (n= 7), and NT-ASO injected *Kcnq4* $^{W277S/+}$ (n= 6) mice at 3 (d), 5 (e), and 7 (f) weeks of age. Data are presented as mean ± SDs. Two-way ANOVA tests with Bonferroni multiple comparison correction were conducted to determine statistical significance. ns: not significant.

4. ASO-123 delivery into the inner ear of *Kcnq4* $^{W277S/+}$ mice promotes outer hair cell survival and improves its function.

We previously demonstrated that hearing loss in *Kcnq4* $^{W277S/+}$ mice is primarily due to the degenration of OHCs, without prominent disorganization of stereocilia bundle or deterioration of IHCs and spiral ganglion neurons [12]. Therefore, since ASO-123 prevented hearing loss in *Kcnq4* $^{W277S/+}$ mice, we further evaluated the survival of OHCs in ASO-123 injected *Kcnq4* $^{W277S/+}$ mice at 7 weeks of age using Myo7a as a marker for hair cells (Figure 9). Consistent with the previous study, untreated *Kcnq4* $^{W277S/+}$ mice showed marked degeneration of OHCs, particularly in the mid and basal turn of the cochlea at 7 weeks. No significant differences were observed in the number of IHCs between WT and *Kcnq4* $^{W277S/+}$ mice. In ASO-123 injected samples, OHC survival in the apical and mid turns significantly increased compared to untreated *Kcnq4* $^{W277S/+}$ mice. In the basal turn of the cohclea, OHC survival tended to increase in ASO-123 treated mice compared to untreated mice, although this trend did not reach statistical significance. This limitied improvement in OHC survival in the basal turn may expalin the minimal enhancement of DPOAE thresholds in high-frequency regions at 7 weeks. Overall, these results indicate that in vivo ASO-123 delivery facilitated OHC survival in low and mid-frequency regions of the cochlea.

To evaluate the electrophysiologic funtion of OHCs treated with ASO-123, we performed whole-cell patch clamping analysis on OHCs from the cochleae of WT, untreated *Kcnq4*$^{W277S/+}$, and ASO-123 (15 μg) treated *Kcnq4*$^{W277S/+}$ mice at P28 (Figure 10A). First, voltage-dependent activation kinetics were obtained after hyperpolarizing and depolarizing voltage steps, and tail currents were recored at -40mV (Figure 10B). As a reuslt, outward potassium currents were significantly reduced and depleted in *Kcnq4*$^{W277S/+}$ mice compared to WT mice. Following ASO-123 treatment, outward currents displayed an increasing trend compared to control *Kcnq4*$^{W277S/+}$ mice although this change did not reach statistical significance (Figure 10C). Resting membrane potentials (RMP) of OHCs were also measured, revealing that *Kcnq4*$^{W277S/+}$ mice exhibited more depolarized RMP compared to WT mice, while ASO-123 treated *Kcnq4*$^{W277S/+}$ mice displayed more hyperpolarized RMP, with values indistinguishable from those of WT mice (Figure 10D). Additionally, channel sensitivity, measured by relative conductance (G/G_{max}), indicated that ASO-123 treatment markedly improved sensitivity and significantly shifted the half-maximum activation voltage ($V_{1/2}$) to a more hyperpolarized state compared to untreated

Kcnq4$^{W277S/+}$ mice (Figure 10E). Collectively, these findings demonstrate that ASO-123 delivery partially restored OHC electrophysiologic function in *Kcnq4*$^{W277S/+}$ mice.

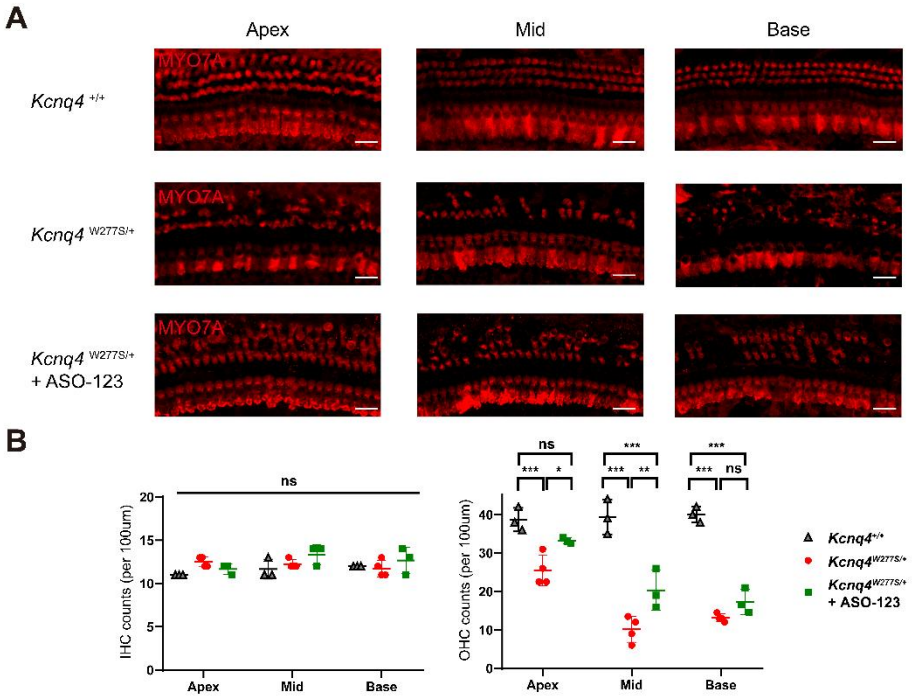

Figure 9. ASO-123 delivery improves OHC survival in *Kcnq4* $^{W277S/+}$ mice. (a) Representative confocal images of whole-mount cochleae stained with Myo7a from *Kcnq4*$^{+/+}$, untreated *Kcnq4*$^{W277S/+}$, and ASO-123 treated *Kcnq4*$^{W277S/+}$ mice at 7 weeks of age. Scale bar = 20 μm. (b) Quantification of the number of IHCs (left) and OHCs (right) across three cochlear turns in the three groups. Data are presented as mean ± SDs. Two-way ANOVA with Bonferroni multiple comparison corrections were conducted to determine statistical significance. ns: not significant; * $P < 0.05$; ** $P < 0.01$; *** $P < 0.001$.

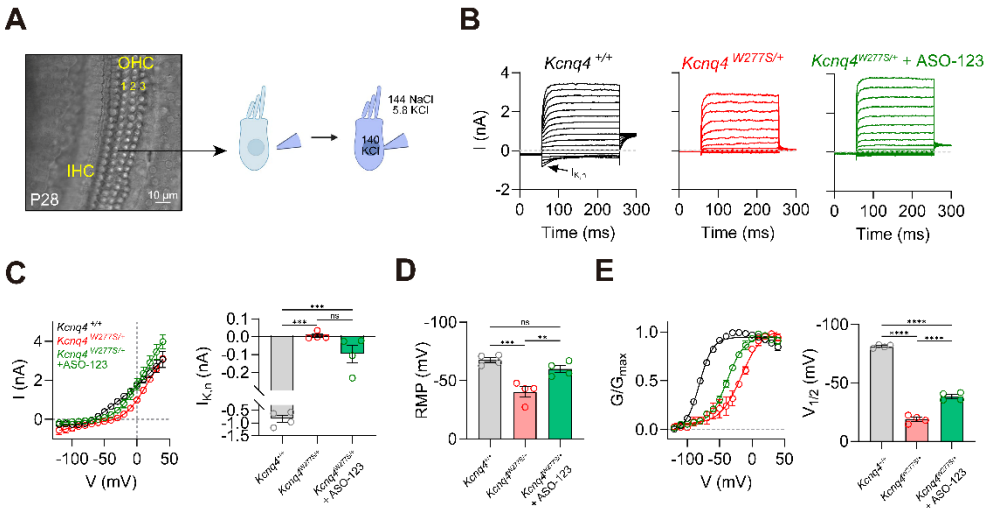

Figure 10. ASO-123 improves Kcnq4 channel function in OHCs of *Kcnq4* $^{W277S/+}$ mice. (a) Schematic illustration of whole-cell patch clamping experiments on OHCs from ex-vivo cochlea at P28. (b) Representative whole-cell current traces of OHCs from the three conditions (*Kcnq4*$^{+/+}$, *Kcnq4*$^{W277S/+}$, and ASO-123 15μg treated *Kcnq4*$^{W277S/+}$ mice). (c) Voltage-dependent activation curves derived from tail currents of whole-cell recording fitted by the Boltzman equation (left) and outward potassium currents derived from these activation curves across the three conditions (right). One-way ANOVA test with Bonferroni's multiple comparison corrections was conducted to determine statistical significance ns: not significant; * $P < 0.05$; ** $P < 0.01$; *** $P < 0.001$. (d) Bar plots presenting the resting membrane potentials of OHCs obtained from the three conditions. One-way ANOVA test with Bonferroni's multiple comparison corrections was conducted to determine statistical significance ns: not significant; * $P < 0.05$; ** $P < 0.01$; *** $P < 0.001$. (e) Relative channel conductance (G/G_{max}) fitted using the Boltzman equation (left) and half-maximum activation voltage ($V_{1/2}$) calculated from the curves across the three conditions (right). One-way ANOVA test with Bonferroni's multiple comparison corrections was conducted to determine statistical significance ns: not significant; * $P < 0.05$; ** $P < 0.01$; *** $P < 0.001$.

5. Transcriptomic alterations reflect efficacy and safety of ASO treatment in *Kcnq4*$^{W277S/+}$ mice.

To comprehensively evaluate transcriptomic changes following ASO administration in *Kcnq4* $^{W277S/+}$ mice, we conducted RNA-sequencing of cochleae from non-injected *Kcnq4*$^{+/+}$, *Kcnq4*$^{W277S/+}$, NT-ASO (15μg)-treated, and ASO-123 (15μg)-treated *Kcnq4*$^{W277S/+}$ mice at P28. ASO injections were performed between P1-3 via the RWM approach. Principal component analysis of the RNA-sequencing data revealed distinct transcriptomic profiles, with replicates from ASO-123 injected *Kcnq4*$^{W277S/+}$ mice clustering closely with *Kcnq4*$^{+/+}$ mice, while untreated and NT-ASO injected *Kcnq4*$^{W277S/+}$ exhibited transcriptomic features more distant from *Kcnq4*$^{+/+}$ mice (Figure 11A). Differentially expressed gene (DEG) analysis (significance deteremined as Benjamini-Hochberg adjusted $P < 0.05$) showed substantial transcriptomic changes in ASO-123-treated *Kcnq4*$^{W277S/+}$ mice compared to untreated and NT-ASO-treated controls. Minimal DEGs were observed between ASO-123-treated *Kcnq4*$^{W277S/+}$ and *Kcnq4*$^{+/+}$ mice (Figure 11B). These findings suggest that ASO-123 effectively restores the transcriptomic profile in *Kcnq4*$^{W277S/+}$ mice. To further assess the biological processes implicated by DEGs, we performed hierarchial clustering of significant DEGs and identified four clusters (Figure 11C). Cluster 2 DEGs were upregulated in untreated and NT-ASO treated *Kcnq4*$^{W277S/+}$ mice and associated with cell cycle and nuclear division, suggesting a compensatory response to cellular degeneration. Cluster 3 DEGs, which were downregulated in untreated and NT-ASO treated *Kcnq4*^{W277S} mice, encompass genes restored following ASO-123 treatment. These genes are involved in cillium assembly, microtubule bundle formation, and regulation of membrane potential. Proper cilium assembly and microtubule bundle formation are associated with hair cell polarity and OHC electromotility [52,53], while Kcnq4 function is essential for OHC membrane potential regulation. Cluster4 DEGs exhibit similar expression levels between untreated and ASO-123 treated *Kcnq4*$^{W277S/+}$ mice and were involved in innate immune response and anti-viral responses, suggesting that ASO-123 did not provoke a marked innate immune response (Figure 11D). Additionally, Gene Set Variation Analysis (GSVA) was performed to confirm functional restoration at the individual sample level (Figure 11E). GSVA revealed that genes involved in potassium ion transport (GO:0006813) and hearing maintenance [44] were coordinately downregulated in untreated and NT-ASO treated *Kcnq4*$^{W277S/+}$ mice but recovered following ASO-123 treatment. Collectively, these findings confirm that ASO-123

restores various biological processes required for hearing maintenance without triggering significant innate immune response.

Since ASO can ellicit in vivo toxicity by activating innate immunity, particularly via Toll-like receptor (TLR) 3,7, and 9 signaling pathways [54-56], we assessed the expression levels of representative target genes from these pathways. No significant differences were observed in TLR target gene expression across untreated, NT-ASO-treated, and ASO-123-treated *Kcnq4*$^{W277S/+}$ mice (Figure 11F). We also examined the expression levels of potential off-target genes, including *Habp4* from in-silico prediction (Table 2) and four genes from the Kcnq family. The expression of these genes remained similar across untreated, NT-ASO, and ASO-123 treated *Kcnq4*$^{W277S/+}$ mice, demonstrating the high specificity of ASO-123 (Figure 11G). Overall, these findings endorse the safety of ASO-123 treatment in the inner ear.

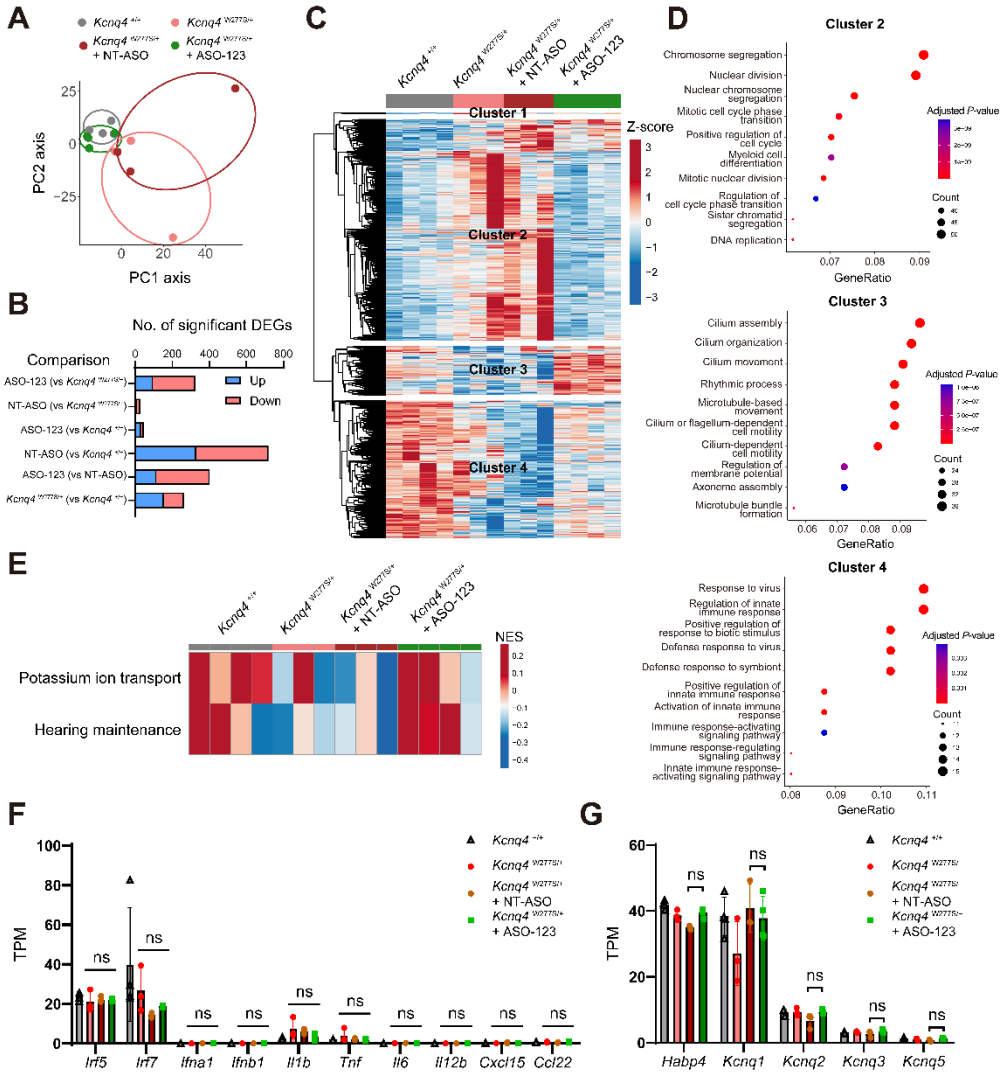

Figure 11. Transcriptomic alterations following ASO treatment in *Kcnq4*$^{W277S/+}$ mice. (a) Principal Component Analysis (PCA) plot of RNA-sequencing data from the four groups (*Kcnq4*$^{+/+}$, *Kcnq4*$^{W277S/+}$, *Kcnq4*$^{W277S/+}$ + NT-ASO 15μg, and *Kcnq4*$^{W277S/+}$ + ASO-123 15μg). (b) Bar plot showing the number of significant differentially expressed genes (DEGs) (Benjamini-Hochberg adjusted $P < 0.05$) between the indicated groups. NT-ASO, *Kcnq4*$^{W277S/+}$ + NT-ASO 15μg; ASO-123, *Kcnq4*$^{W277S/+}$ + ASO-123 15μg. (c) Heatmap of Z-scored, normalized expression levels of significant DEGs (Benjamini-Hochberg adjusted $P < 0.05$) across all comparisons.

Hierarchial clustering was performed to identify DEG clusters. (d) Top 10 significant Gene Ontology (GO) biological process terms (Benjamini-Hochberg adjusted $P < 0.05$), ranked by gene ratio (gene count within a term dividied by total genes), enriched in each DEG cluster. Colors represent adjusted *P*-values, and sizes correspond to the number of DEGs within each GO term. (e) Heatmap representing Gene Set Variation Analysis (GSVA) results. Columns represent samples, and rows indicate tested gene sets, with colors indicating normalized enrichment scores (NES). (f) Bar plots displaying the Transcripts Per Million (TPM) values of representative target genes from the Toll-like receptor 3,7, and 9 signaling pathways across the four groups. Data are shown as mean ± SDs. Two-way ANOVA with Bonferroni's multiple comparison corrections determined statistical significance. ns, not significant. (g) Bar plots showing TPM values of the potential off-target genes across the four groups. Data are presented as mean ± SDs. Two-way ANOVA with Bonferroni's multiple comparison corrections were performed to determine statistical significance. ns, not significant.

6. ASO-123 exhibits allele preference for human *KCNQ4* p.W276S over *KCNQ4* WT.

Since the region of mouse *Kcnq4* exon5 surrounding the target mutation (*Kcnq4* c.830G>C; p.W277S, homologous to human *KCNQ4* c.827G>C; p.W276S) and the ASO-123 target sequence are highly conserved between human and mouse (Figure 12A), we investigated whether ASO-123 exhibits a similar allele preference for the *KCNQ4* p.W276S mutation over *KCNQ4* WT, resembling that in mouse *Kcnq4*. To validate this, HEK293T cells were co-transfected with either *KCNQ4* WT or W276S and treated with NT-ASO or ASO-123 (both in 150nM). Protein expression was assessed 48 hours post-transfection to determine allele preference (Figure 12B). Quantification of band intensities revealed that ASO-123 significantly reduced KCNQ4 W276S expression while relatively preserving KCNQ4 WT expression compared to NT-ASO treated samples (Figure 12C). Further dose-response analysis demonstrated pronounced preferential knock-down of KCNQ4 W276S over KCNQ4 WT, as reflected in the IC_{50} values (IC_{50} for KCNQ4 W276S: 71.26nM; IC50 for KCNQ4 WT: 173.8nM) (Figure 12D-E). Taken together, these findings indicate ASO-123's strong allele preference for human *KCNQ4* W276S over *KCNQ4* WT and highlight its potential as a targeted therapeutic approach for human DFNA2 caused by the c.827G>C mutation with further optimization.

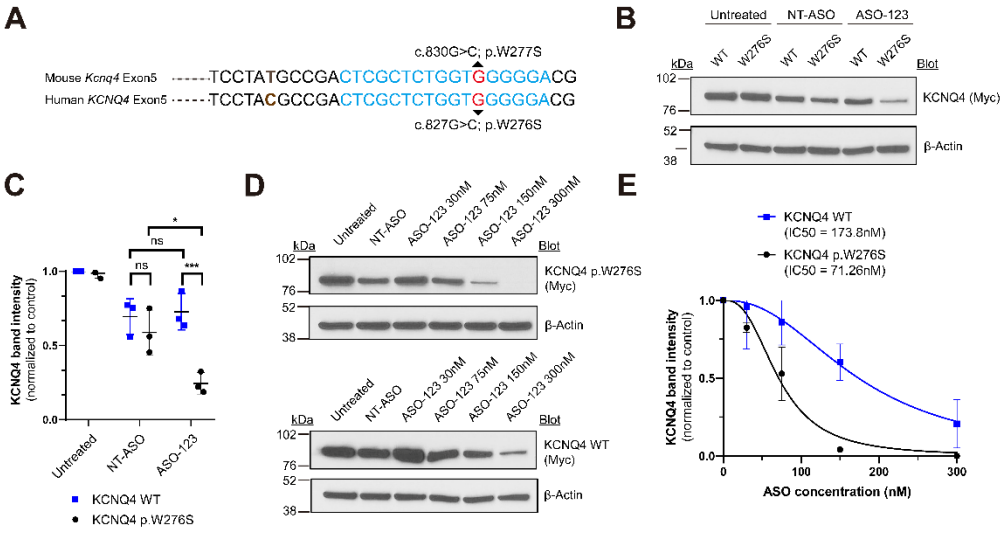

Figure 12. ASO-123 displays allele preference for human *KCNQ4* p.W276S over *KCNQ4* WT. (a) Alignment of part of human *KCNQ4* and mouse *Kcnq4* exon5 sequences surrounding the target mutation (c.827G>C; p.W276S in human *KCNQ4*). The ASO-123 target sequence and target mutation are highlighted in blue and red, respectively, with a mismatched base shown in brown. (b) Representative western blot images following treatment with NT-ASO or ASO-123 (150nM) for KCNQ4 WT or W276S. (c) KCNQ4 WT and W276S protein band intensities normalized to β-Actin and then to untreated KCNQ4 WT intensities (n=3). Data are presented as mean ± SDs. Two-way ANOVA with Tukey's multiple comparison corrections were conducted to determine statistical significance. ns, not significant; * $P < 0.05$; ** $P < 0.01$; *** $P < 0.001$. (d) Representative western blot images after treatment with NT-ASO or ASO-123 across a range of concentrations (30nM to 300nM) for KCNQ4 WT or W276S. (e) Dose-response curves of ASO-123 for KCNQ4 W276S and WT, normalized to β-Actin and then to untreated controls (n=3). Data are presented as mean ± SDs.

III. DISCUSSION

In this study, we utilized an allele-specific ASO strategy to alleviate progressive hearing loss in *Kcnq4* $^{W277S/+}$ mice, which model the human DFNA2 phenotype. Through in vitro screening, we identified a promising allele-specific ASO (ASO-123) that selectively targets the *Kcnq4* W277S allele while sparing the WT allele and assessed its safety and off-target profile. We subsequently administered this ASO to *Kcnq4* $^{W277S/+}$ mice at P1-P3 via RWM injection and observed notable improvement in progressive hearing loss, particularly in the low and mid-frequency ranges, lasting until 7 weeks post-injection, along with enhanced OHC survival and function. Notably, to the best of our knowledge, this study represents the first study demonstrating the therapeutic potential of an RNase-H1 dependent allele-specific ASO approach for treating hereditary hearing loss.

Notably, we observed a significant improvement in OHC survival in low and mid-frequency regions, which was not achieved with the CRISPR-Cas9-based approach previously used in the same model [12]. This finding emphasizes the enhanced efficiency of allele-specific ASOs in targeting the Kcnq4 W277S mutation (28 – 30%) compared to CRISPR-Cas9, which generally exhibits an efficiency of no more than 20% at both the genomic DNA and cDNA levels [12,18,57]. Furthermore, since ASO primarily targets mRNA and exhibit effects over relatively short periods, this approach may potentially circumvent safety concerns regarding permanent DNA damages to targeted and off-targeted regions inflicted by CRISPR-Cas9.

While the allele-specific ASO significantly mitigated hearing loss in the low and mid-frequency regions, improvements in high-frequency regions were limited compared to other frequencies. This finding might be attributable to the spatiotemporal regulation of *Kcnq4* expression, which begins in the basal turn at embryonic days 18.5 and progressively moves towards the apical turn in mice [58]. Therefore, the timing of ASO delivery during the P1-P3 period may be too late to effectively restore OHC function and survival in the basal turn region. Moreover, since OHC degeneration in *Kcnq4*$^{W277S/+}$ mice starts in the basal turn and spreads toward the apical turn, the efficiency of the delivered ASO might not be adequate to counteract the dominant-negative effects of mutant Kcnq4 in the basal turn. Future studies could enhance hearing improvement in high-frequency regions and broaden the therapeutic index by optimizing ASO characteristics, such as improving allele discrimination through stereopure phosphorothioate bonds [59] or using a phosphoryl guanidine-containing backbone [60], and increasing gapmer ASO

tolerability by substituting phosphodiester bonds for phosphorothioate bonds in specific wing positions [61].

Through deep sequencing of *Kcnq4* transcripts, we found that ASO-123 injection preferentially knocked down mutant transcripts over WT transcripts. However, when considering the expression levels of total *Kcnq4* mRNA from ASO-injected *Kcnq4*$^{W277S/+}$ mice, we observed some suppression of *Kcnq4* WT transcripts, particularly in those injected with 30 μg of ASO-123. However, given that the probability of loss intolerance (pLI) score for the *Kcnq4* gene is 0.02 (gnomAD v4.1.0) [62], and that a heterozygote knock out of *Kcnq4* allele in mice did not result in hearing loss [6], both suggest that *Kcnq4* is unlikely to be haploinsufficient, and a partial reduction of WT transcripts may be tolerable. Nevertheless, determining an administration dose of allele-specific ASO that does not significantly diminish the expression of WT transcripts is essential for ensuring effective and safe treatment.

Serial audiologic assessments indicated that the therapeutic effects of ASO-123 persisted for up to 7 weeks post-injection. This relatively short duration of ASO treatment is attributed to the gradual consumption and degradation of RNase-H1 dependent ASO when it binds to its target transcript. Therefore, to sustain the therapeutic effects of RNase-H1-dependent ASO, repeated administration at regular intervals is necessary. In line with this, several ASO drugs for clinical use require regular dosing every 2 to 3 months as part of maintenance therapy [27,28,33]. In this study, we utilized RWM approach for localized ASO delivery in the inner ear, as it has previously demonstrated superior pharmacokinetic efficiency compared to other techniques such as intratympanic injection or topical-tympanic membrane application [34]. However, in clinical settings involving human patients, frequent and multiple RWM injections are impractical due to the need for invasive surgical procedures (either via transcanal or transmastoid approaches). Thus, it is crucial to explore more reliable and non-invasive methods for delivering ASO to the inner ear for future human applications.

IV. CONCLUSION

Among autosomal dominant non-syndromic hearing loss cases, approximately 85% are caused by missense mutation [63]. Furthermore, regarding *KCNQ4*-associated autosomal dominant hearing loss, most deafness-associated variants are missense variants, the majority of which are presumed to be dominant-negative rather than due to haploinsufficiency [4,9]. Additionally, many deafness-causing genes, including *KCNQ4*, are primarily involved in the development, homeostasis, and function of hair cells [64], making them effective targets for ASO therapy. Collectively, these facts underscore the broad applicability of the allele-specific ASO modality in treating hereditary hearing loss. Overall, our study provides evidence for the therapeutic potential of the allele-specific ASO approach in genetic hearing loss and serves as a blueprint for future clinical translation.

References

1. Chadha, S., Kamenov, K. & Cieza, A. The world report on hearing, 2021. *Bull World Health Organ* **99**, 242-242a (2021).
2. Morton, C.C. & Nance, W.E. Newborn hearing screening--a silent revolution. *N Engl J Med* **354**, 2151-2164 (2006).
3. Rim, J.H.*, et al.* Differential genetic diagnoses of adult post-lingual hearing loss according to the audiogram pattern and novel candidate gene evaluation. *Hum Genet* **141**, 915-927 (2022).
4. Oh, K.S.*, et al.* Overlooked KCNQ4 variants augment the risk of hearing loss. *Exp Mol Med* **55**, 844-859 (2023).
5. Kubisch, C.*, et al.* KCNQ4, a novel potassium channel expressed in sensory outer hair cells, is mutated in dominant deafness. *Cell* **96**, 437-446 (1999).
6. Kharkovets, T.*, et al.* Mice with altered KCNQ4 K+ channels implicate sensory outer hair cells in human progressive deafness. *Embo j* **25**, 642-652 (2006).
7. Lee, S.Y.*, et al.* Novel KCNQ4 variants in different functional domains confer genotype- and mechanism-based therapeutics in patients with nonsyndromic hearing loss. *Exp Mol Med* **53**, 1192-1204 (2021).
8. Kamada, F.*, et al.* A novel KCNQ4 one-base deletion in a large pedigree with hearing loss: implication for the genotype-phenotype correlation. *J Hum Genet* **51**, 455-460 (2006).
9. Jung, J.*, et al.* Rare KCNQ4 variants found in public databases underlie impaired channel activity that may contribute to hearing impairment. *Exp Mol Med* **51**, 1-12 (2019).
10. Coucke, P.J.*, et al.* Mutations in the KCNQ4 gene are responsible for autosomal dominant deafness in four DFNA2 families. *Hum Mol Genet* **8**, 1321-1328 (1999).
11. Van Camp, G.*, et al.* A mutational hot spot in the KCNQ4 gene responsible for autosomal dominant hearing impairment. *Hum Mutat* **20**, 15-19 (2002).
12. Noh, B.*, et al.* In vivo outer hair cell gene editing ameliorates progressive hearing loss in dominant-negative Kcnq4 murine model. *Theranostics* **12**, 2465-2482 (2022).
13. Lv, J.*, et al.* AAV1-hOTOF gene therapy for autosomal recessive deafness 9: a single-arm trial. *Lancet* **403**, 2317-2325 (2024).
14. Wang, H.*, et al.* Bilateral gene therapy in children with autosomal recessive deafness 9: single-arm trial results. *Nat Med* **30**, 1898-1904 (2024).
15. Mendia, C.*, et al.* Clarin-2 gene supplementation durably preserves hearing in a model of progressive hearing loss. *Mol Ther* **32**, 800-817 (2024).
16. Shubina-Oleinik, O.*, et al.* Dual-vector gene therapy restores cochlear amplification and auditory sensitivity in a mouse model of DFNB16 hearing loss. *Sci Adv* **7**, eabi7629 (2021).
17. Ivanchenko, M.V.*, et al.* Mini-PCDH15 gene therapy rescues hearing in a mouse model of Usher syndrome type 1F. *Nat Commun* **14**, 2400 (2023).
18. Tao, Y.*, et al.* Treatment of monogenic and digenic dominant genetic hearing loss by CRISPR-Cas9 ribonucleoprotein delivery in vivo. *Nat Commun* **14**, 4928 (2023).
19. György, B.*, et al.* Allele-specific gene editing prevents deafness in a model of dominant progressive hearing loss. *Nat Med* **25**, 1123-1130 (2019).
20. Fu, Y.*, et al.* High-frequency off-target mutagenesis induced by CRISPR-Cas nucleases in human cells. *Nat Biotechnol* **31**, 822-826 (2013).
21. Lin, Y.*, et al.* CRISPR/Cas9 systems have off-target activity with insertions or deletions between target DNA and guide RNA sequences. *Nucleic Acids Res* **42**, 7473-7485 (2014).

22. Shin, H.Y., *et al.* CRISPR/Cas9 targeting events cause complex deletions and insertions at 17 sites in the mouse genome. *Nat Commun* **8**, 15464 (2017).
23. Kosicki, M., Tomberg, K. & Bradley, A. Repair of double-strand breaks induced by CRISPR-Cas9 leads to large deletions and complex rearrangements. *Nat Biotechnol* **36**, 765-771 (2018).
24. Nelson, C.E., *et al.* Long-term evaluation of AAV-CRISPR genome editing for Duchenne muscular dystrophy. *Nat Med* **25**, 427-432 (2019).
25. Lek, A., *et al.* Death after High-Dose rAAV9 Gene Therapy in a Patient with Duchenne's Muscular Dystrophy. *N Engl J Med* **389**, 1203-1210 (2023).
26. Verdera, H.C., Kuranda, K. & Mingozzi, F. AAV Vector Immunogenicity in Humans: A Long Journey to Successful Gene Transfer. *Mol Ther* **28**, 723-746 (2020).
27. Kim, J., *et al.* Patient-Customized Oligonucleotide Therapy for a Rare Genetic Disease. *N Engl J Med* **381**, 1644-1652 (2019).
28. Kim, J., *et al.* A framework for individualized splice-switching oligonucleotide therapy. *Nature* **619**, 828-836 (2023).
29. Chen, X., *et al.* Antisense oligonucleotide therapeutic approach for Timothy syndrome. *Nature* **628**, 818-825 (2024).
30. Dindot, S.V., *et al.* An ASO therapy for Angelman syndrome that targets an evolutionarily conserved region at the start of the UBE3A-AS transcript. *Sci Transl Med* **15**, eabf4077 (2023).
31. Shao, Y., *et al.* Antisense oligonucleotide therapy in a humanized mouse model of MECP2 duplication syndrome. *Sci Transl Med* **13**(2021).
32. Viengkhou, B., *et al.* Interferon-α receptor antisense oligonucleotides reduce neuroinflammation and neuropathology in a mouse model of cerebral interferonopathy. *J Clin Invest* **134**(2024).
33. Ziegler, A., *et al.* Antisense oligonucleotide therapy in an individual with KIF1A-associated neurological disorder. *Nat Med* (2024).
34. Lentz, J.J., *et al.* Direct Delivery of Antisense Oligonucleotides to the Middle and Inner Ear Improves Hearing and Balance in Usher Mice. *Mol Ther* **28**, 2662-2676 (2020).
35. Lentz, J.J., *et al.* Rescue of hearing and vestibular function by antisense oligonucleotides in a mouse model of human deafness. *Nat Med* **19**, 345-350 (2013).
36. Gee, H.Y., Tang, B.L., Kim, K.H. & Lee, M.G. Syntaxin 16 binds to cystic fibrosis transmembrane conductance regulator and regulates its membrane trafficking in epithelial cells. *J Biol Chem* **285**, 35519-35527 (2010).
37. Li, H. & Durbin, R. Fast and accurate short read alignment with Burrows-Wheeler transform. *Bioinformatics* **25**, 1754-1760 (2009).
38. Bolger, A.M., Lohse, M. & Usadel, B. Trimmomatic: a flexible trimmer for Illumina sequence data. *Bioinformatics* **30**, 2114-2120 (2014).
39. Kim, D., Langmead, B. & Salzberg, S.L. HISAT: a fast spliced aligner with low memory requirements. *Nat Methods* **12**, 357-360 (2015).
40. Liao, Y., Smyth, G.K. & Shi, W. featureCounts: an efficient general purpose program for assigning sequence reads to genomic features. *Bioinformatics* **30**, 923-930 (2014).
41. Love, M.I., Huber, W. & Anders, S. Moderated estimation of fold change and dispersion for RNA-seq data with DESeq2. *Genome Biol* **15**, 550 (2014).
42. Xu, S., *et al.* Using clusterProfiler to characterize multiomics data. *Nat Protoc* **19**, 3292-3320 (2024).
43. Hänzelmann, S., Castelo, R. & Guinney, J. GSVA: gene set variation analysis for

microarray and RNA-seq data. *BMC Bioinformatics* **14**, 7 (2013).
44. Sun, G.*, et al.* Single-cell transcriptomic atlas of mouse cochlear aging. *Protein Cell* **14**, 180-201 (2023).
45. Kechin, A., Boyarskikh, U., Kel, A. & Filipenko, M. cutPrimers: A New Tool for Accurate Cutting of Primers from Reads of Targeted Next Generation Sequencing. *J Comput Biol* **24**, 1138-1143 (2017).
46. Callahan, B.J.*, et al.* DADA2: High-resolution sample inference from Illumina amplicon data. *Nat Methods* **13**, 581-583 (2016).
47. Rinaldi, C. & Wood, M.J.A. Antisense oligonucleotides: the next frontier for treatment of neurological disorders. *Nat Rev Neurol* **14**, 9-21 (2018).
48. Shen, W.*, et al.* Chemical modification of PS-ASO therapeutics reduces cellular protein-binding and improves the therapeutic index. *Nat Biotechnol* **37**, 640-650 (2019).
49. Finkel, R.S.*, et al.* Nusinersen versus Sham Control in Infantile-Onset Spinal Muscular Atrophy. *N Engl J Med* **377**, 1723-1732 (2017).
50. Benson, M.D.*, et al.* Inotersen Treatment for Patients with Hereditary Transthyretin Amyloidosis. *N Engl J Med* **379**, 22-31 (2018).
51. Mathiesen, B.K.*, et al.* Delivery of gene therapy through a cerebrospinal fluid conduit to rescue hearing in adult mice. *Sci Transl Med* **15**, eabq3916 (2023).
52. Kirjavainen, A., Laos, M., Anttonen, T. & Pirvola, U. The Rho GTPase Cdc42 regulates hair cell planar polarity and cellular patterning in the developing cochlea. *Biol Open* **4**, 516-526 (2015).
53. Bai, J.P.*, et al.* Prestin surface expression and activity are augmented by interaction with MAP1S, a microtubule-associated protein. *J Biol Chem* **285**, 20834-20843 (2010).
54. Toonen, L.J.A.*, et al.* Intracerebroventricular Administration of a 2'-O-Methyl Phosphorothioate Antisense Oligonucleotide Results in Activation of the Innate Immune System in Mouse Brain. *Nucleic Acid Ther* **28**, 63-73 (2018).
55. Pollak, A.J.*, et al.* Insights into innate immune activation via PS-ASO-protein-TLR9 interactions. *Nucleic Acids Res* **50**, 8107-8126 (2022).
56. Moazami, M.P.*, et al.* Quantifying and mitigating motor phenotypes induced by antisense oligonucleotides in the central nervous system. *Mol Ther* (2024).
57. Zhu, W.*, et al.* Targeted genome editing restores auditory function in adult mice with progressive hearing loss caused by a human microRNA mutation. *Sci Transl Med* **16**, eadn0689 (2024).
58. Beisel, K.W.*, et al.* Differential expression of KCNQ4 in inner hair cells and sensory neurons is the basis of progressive high-frequency hearing loss. *J Neurosci* **25**, 9285-9293 (2005).
59. Iwamoto, N.*, et al.* Control of phosphorothioate stereochemistry substantially increases the efficacy of antisense oligonucleotides. *Nat Biotechnol* **35**, 845-851 (2017).
60. Kandasamy, P.*, et al.* Impact of guanidine-containing backbone linkages on stereopure antisense oligonucleotides in the CNS. *Nucleic Acids Res* **50**, 5401-5423 (2022).
61. Tran, H.*, et al.* Suppression of mutant C9orf72 expression by a potent mixed backbone antisense oligonucleotide. *Nat Med* **28**, 117-124 (2022).
62. Chen, S.*, et al.* A genomic mutational constraint map using variation in 76,156 human genomes. *Nature* **625**, 92-100 (2024).
63. Sloan-Heggen, C.M.*, et al.* Comprehensive genetic testing in the clinical evaluation of 1119 patients with hearing loss. *Hum Genet* **135**, 441-450 (2016).
64. Petit, C., Bonnet, C. & Safieddine, S. Deafness: from genetic architecture to gene therapy.

Nat Rev Genet **24**, 665-686 (2023).

Abstract in Korean

KCNQ4 연관 난청 유발 대립유전자에 특이적인 안티센스 올리고핵산 치료제 개발 및 최적화

난청은 가장 흔한 감각기 질환이며 유전적 요인은 난청의 발병 원인 중 큰 부분을 차지하고 있다. *KCNQ4*는 전위의존성 칼륨채널로 내이의 외유모세포에서 높게 발현하는 유전자이며 동아시아에서 상염색체 우성 형태로 발병하는 유전성 난청의 중요한 원인 유전자로 알려져 있고 돌연변이가 발생할 시 상염색체 우성 진행성 난청(DFNA2)를 일으키는 것으로 알려져 있다. 난청과 연관된 많은 *KCNQ4* 변이 중 *KCNQ4* p.W276S (c.G827C) 변이는 dominant-negative 효과로 난청을 일으키는 것이 알려져 있으며 KCNQ4 채널 내에서 돌연변이가 호발하는 hot spot region에 위치한 변이이다. 이처럼 *KCNQ4*로 인한 난청은 유병율이 높지만 현재까지 효과적인 생물학적 치료 방법이 개발되지 못하였다. 이에 본 연구에서는 *KCNQ4*의 dominant-negative 효과를 보이는 돌연변이를 타겟으로 하는 대립유전자 특이적인 안티센스 올리고핵산 (Antisense oligonucleotides, ASO) 치료제를 개발하고 최적화하고자 하였다.

우선 사람의 *KCNQ4* p.W276S 변이에 상동하는 마우스의 *Kcnq4* p.W277S 변이를 타깃으로 하는 9종류의 대립유전자 특이적인 안티센스 올리고핵산 치료제를 디자인하였고 이들의 효과를 세포 수준에서 확인하였다. 이를 통해 두종류의 ASO를 후보 물질로 선정하고 이들의 농도 의존적인 효과 및 독성유발 가능성 평가를 통하여 한 종류의 ASO (ASO-123)을 동물실험을 위한 물질로 최종 선정하였다. 선정된 ASO는 *Kcnq4* p.W277S 변이를 이형접합으로 가지는 마우스에서 생후 1-3일 사이에 정원창을 통해 주입하였고 약 4주후에 *Kcnq4* p.W277S 돌연변이를 가진 대립유전자의 발현이 정상 대립유전자 대비 통계적으로 유의하게 억제되는 것을 확인하였다. 이러한 유전자 수준에서 발현 조절은 ASO 주입하고 약 7주후까지 청력검사 상에서 지연성 난청을 완화시키는 결과를 보였고 외유모세포의 생존 및 전기생리학적 기능이 개선되는 것을 확인하였다. 본 연구 결과는 유전성 난청 동물모델에서 대립유전자 특이적인 ASO 치료전략의 효용성을 종합적으로 평가한 최초의 연구로 추후 최적화 과정을 통해 실제 사람에서 난청 치료에 ASO가 이용될 수 있다는 가능성을 제시하였다.

핵심되는 말: 난청, 내이, 상염색체 우성, 안티센스 올리고핵산 치료제